

Electronic Supplementary Information to accompany

Single ion anisotropy and exchange coupling in cobalt(II)-radical
complexes: insights from magnetic and *ab initio* studies

Gemma K. Gransbury, Marie-Emmanuelle Boulon, Richard A. Mole, Robert W. Gable,
Boujemaâ Moubaraki, Keith S. Murray, Lorenzo Sorace, Alessandro Soncini*, Colette
Boskovic*

*Email: c.boskovic@unimelb.edu.au, asoncini@unimelb.edu.au

[†]School of Chemistry, University of Melbourne, Victoria 3010, Australia

[¶]UdR INSTM and Department of Chemistry “U. Schiff”, University of Florence, 50019 Sesto
Fiorentino (FI), Italy

[§]Australian Nuclear Science and Technology Organisation, Locked Bag 2001, Kirrawee DC,
New South Wales 2232, Australia

[‡]School of Chemistry, Monash University, Clayton 3800, Australia

Contents:

1. Synthetic procedures	S3
2. Crystal images.....	S6
3. Thermogravimetric analysis.....	S7
4. Infrared spectroscopy.....	S7
5. Crystallographic study	S8
6. Powder X-ray diffraction	S15
7. Electronic absorption spectroscopy	S17
8. EPR spectroscopy	S22
9. Magnetic data.....	S24
10. Inelastic neutron scattering	S26
11. Theoretical calculations on Co(II) analogues	S32
12. Theoretical calculations on Co(II)-semiquinonate.....	S39
13. Two-state model of magnetic susceptibility	S49
14. Intermolecular interactions	S50
15. Input coordinates for theoretical calculations	S53
16. References.....	S69

1. Synthetic procedures

Materials and Methods.

All chemicals were of reagent grade and used as received. Reactions were performed in an aerobic atmosphere unless stated otherwise. Tris(6-methyl-2-pyridylmethyl)amine was synthesized based on a literature procedure with recrystallization from diethyl ether.¹ The compounds 6-methyl-2-aminomethylpyridine and the precursor 6-formaldoximo-2-methylpyridine were synthesized by the literature procedures.^{2,3}

[Co(Me₃tpa)(Br₄cat)] (1) and [Zn(Me₃tpa)(Br₄cat)], (1-Zn). Compounds **1** and **1-Zn** were synthesized according to the literature procedure and purity was established by combustion analysis, infrared (IR), powder X-ray diffraction (PXRD) and thermogravimetric analysis (TGA).⁴

[Zn_{0.95}Co_{0.05}(Me₃tpa)(Br₄cat)], (1-Co_{0.05}). The synthesis of **1-Co_{0.05}** was based on the previously reported synthesis of **1** and **1-Zn**.⁴ Tris(6-methyl-2-pyridylmethyl)amine (Me₃tpa, 0.333 g, 1.00 mmol) was added to a solution of ZnCl₂ (0.130 g, 0.955 mmol) and CoCl₂·6H₂O (11.8 mg, 0.496 mmol) in methanol (75 mL). After 10 minutes of stirring at room temperature, a solution of tetrabromocatechol (Br₄catH₂, 0.426 g, 1.00 mmol) in methanol (10 mL), deprotonated with triethylamine (0.280 mL, 2.01 mmol), was added dropwise. The precipitate was collected by vacuum filtration, washed with methanol, diethyl ether and air dried. The crude product was recrystallized from hot DMF/diethyl ether to give **1-Co_{0.05}** as a microcrystalline orange powder (Yield: 0.490 g, 60%). The bulk sample product was confirmed to be isomorphous with **1** and **1-Zn** by PXRD (Fig. S10). Single crystals of X-ray diffraction quality were produced by layering a DMF solution with diethyl ether (1:2). Found: C, 39.71; H, 2.92; N, 6.67. Calc. for C₂₇H₂₄N₄O₂Br₄Co_{0.05}Zn_{0.95}: C, 39.49; H, 2.95; N, 6.82%.

[Co(Me₃tpa)(trop)](PF₆), (2(PF₆)) Tropolone (0.0847 g, 0.694 mmol) was dissolved in methanol (5 mL) and deprotonated with triethylamine (0.061 mL, 0.438 mmol). The

tropolonate solution was added dropwise to a solution of $\text{CoCl}_2 \cdot 6\text{H}_2\text{O}$ (0.146 g, 0.615 mmol) and Me_3tpa (0.200 g, 0.601 mmol) in methanol (20 mL). The reaction mixture was stirred for 5 min at room temperature and then the crude product precipitated with a saturated aqueous solution of potassium hexafluorophosphate (40 mL). The precipitate was collected by vacuum filtration, washed with saturated aqueous potassium hexafluorophosphate solution, water, minimal ice-cold ethanol and diethyl ether and then air dried to give **2(PF₆)** as a pale orange solid (Yield: 0.306 g, 77%). Crystallographic analysis allowed the identification of single crystals of four different phases (*I*, *II*, *III* and *IV*) from toluene. The crude product was recrystallized from toluene and identified as phase *I* by PXRD (Fig. S11). Found: C, 51.07; H, 4.44; N, 8.47; P, 4.71. Calc. for $\text{C}_{28}\text{H}_{29}\text{N}_4\text{O}_2\text{CoPF}_6$: C, 51.15; H, 4.45; N, 8.52; P, 4.71%. TGA data are consistent with no solvation. $\lambda_{\max}(\text{MeCN})/\text{nm}$ 238 ($\epsilon/\text{dm}^3 \text{ mol}^{-1}$ 36 200), 251 (27 600sh), 258 (23 100sh), 277 (9 110sh), 325 (10 900sh), 340 (14 100), 383 (5 610), 401 (4 660sh), 485 (129sh), 526 (108), 560 (87), 595 (43sh), 1077 (11). $\nu_{\max}/\text{cm}^{-1}$ (KBr): 1607m, 1593m, 1580w, 1513m, 1469m, 1453m, 1433m, 1385m, 1363m, 1246w, 1231w, 1165w, 1122w, 1098w, 1038w, 1010w, 972w, 915w, 876w, 840s, 786m, 737w, 698w, 558m, 530w, 406w. m/z 513.1630 [M-PF₆]⁺ calc. for $\text{C}_{28}\text{H}_{29}\text{N}_4\text{O}_2\text{Co}$ 512.1623.

[Zn(Me₃tpa)(trop)](PF₆), (2-Zn(PF₆)). Synthesized as per **2(PF₆)** from Me₃tpa (0.299 g, 0.900 mmol), tropolone (0.110 g, 0.901 mmol) and triethylamine (0.120 mL, 0.860 mmol). The reagent $\text{CoCl}_2 \cdot 6\text{H}_2\text{O}$ was replaced by ZnCl_2 (0.123 g, 0.899 mmol) in **2-Zn(PF₆)**. A larger volume of methanol was used to account for the low solubility of ZnCl_2 . Compound **2-Zn(PF₆)** was recrystallized from toluene to give pale yellow powder (Yield: 0.442 g, 74%). A single crystal obtained from toluene was isomorphous with **2(PF₆)·1.5tol-III** while the bulk sample analyzed as solvent-free and was identified as phase *I* by PXRD (Fig. S11). Found: C, 50.92; H, 4.27; N, 8.59. Calc. for $\text{C}_{28}\text{H}_{29}\text{N}_4\text{O}_2\text{ZnPF}_6$: C, 50.65; H, 4.40; N, 8.44%. $\lambda_{\max}(\text{MeCN})/\text{nm}$ 233 ($\epsilon/\text{dm}^3 \text{ mol}^{-1}$ 37 200sh), 236 (38 300), 238 (37 900sh), 244 (30 000sh), 253 (23 900), 262 (21 400), 274 (9 200), 311 (7 620sh), 327 (16 900), 330 (16 800), 357 (2 9200sh), 365 (3

540sh), 377 (5 610sh), 387 (7 200sh), 394 (8 340). $\nu_{\text{max}}/\text{cm}^{-1}$ (KBr): 1606m, 1594m, 1580w, 1513m, 1468m, 1452m, 1431m, 1411m, 1383m, 1361m, 1247w, 1231w, 1162w, 1125w, 1096w, 1034w, 1013w, 973w, 916w, 900w, 876w, 840s, 789m, 739w, 697w, 558m, 538w, 407w. m/z 517.1457 [M-PF₆]⁺ calc. for C₂₈H₂₉N₄O₂Zn 517.1582.

[Co(Me₃tpa)(dbsq)](PF₆)·C₆H₅CH₃, (3(PF₆)·tol). Compound **3(PF₆)·tol** was synthesized under a nitrogen atmosphere according to the procedure reported by Dei *et al.* and recrystallized from toluene to give a dark green solid (Yield: 1.81 g, 71%).¹ The crystal structure at 100 K and PXRD pattern matched the structure reported previously (Fig. S12). Found C, 59.51; H, 6.21; N, 6.51; P, 3.69. Calc. for C₄₂H₅₂N₄O₂CoPF₆: C, 59.43; H, 6.17; N, 6.60; P, 3.65%. TGA data are consistent with one toluene solvate per molecule, lost over two steps. Centered at 149 °C, 0.39 of a toluene molecule was lost, with the remaining fraction observed as a mass loss centered at 170 °C. $\lambda_{\text{max}}(\text{MeCN})/\text{nm}$ 264 ($\epsilon/\text{dm}^3 \text{ mol}^{-1}$ 13 500), 275 (9 900sh), 298 (9 150sh), 306 (1 030), 354 (2 360sh), 375 (1 470sh), 424 (1 210), 493 (590sh), 537 (773sh), 610 (779 sh), 642 (759sh), 571 (850), 769 (447sh), 866 (274sh), 1037 (43sh). $\nu_{\text{max}}/\text{cm}^{-1}$ (KBr): 1606m, 1579m, 1451m, 1385w, 1354w, 1329w, 1295w, 1243w, 1203w, 1165w, 1119w, 1098w, 1030w, 1009w, 984w, 948w, 842s, 787m, 743m, 699w, 657w, 558m, 494w, 468w. m/z 611.2824 [M-PF₆-tol]⁺ calc. for, C₃₅H₄₄N₄O₂Co 611.2796.

[Zn(Me₃tpa)(dbsq)](PF₆)·C₆H₅CH₃, (3-Zn(PF₆)·tol). Compound **3-Zn(PF₆)·tol** was synthesized based on the literature procedure for **3(PF₆)·tol**.¹ A solution of 3,5-di-*tert*-butylcatechol (0.605 g, 2.72 mmol) in methanol (350 mL) and a solution/suspension of Me₃tpa (0.903 g, 2.72 mmol) and ZnCl₂ (0.370 g, 2.71 mmol) in methanol (50 mL) were degassed by five vacuum/nitrogen cycles. The 3,5-di-*tert*-butylcatechol solution was deprotonated with triethylamine (0.76 mL, 5.4 mmol) and immediately transferred to the zinc/Me₃tpa suspension. The reaction mixture was stirred for 10 min under a nitrogen atmosphere before bubbling with condensed air for 2 h. The product was concentrated under reduced pressure, the crude product was precipitated with a saturated aqueous potassium

hexafluorophosphate solution and collected by vacuum filtration, washed with saturated aqueous potassium hexafluorophosphate solution then water and air dried. The crude product was recrystallized from toluene with hot filtration to give **3-Zn(PF₆)·tol** as dark blue crystals (1.94 g, 84%). Found: C, 59.02; H, 6.18; N, 6.81. Calc. C₄₂H₅₂N₄O₂ZnPF₆: C, 58.98; H 6.13; N 6.55%. $\lambda_{\text{max}}(\text{MeCN})/\text{nm}$ 264 ($\epsilon/\text{dm}^3 \text{ mol}^{-1}$ 14 600), 274 (9 710sh), 302 (8 190sh), 310 (9 640), 346 (1 870), 362 (1 680), 376 (1 660), 427 (79sh), 510 (59sh), 729 (354sh), 771 (375), 869 (253sh). $\nu_{\text{max}}/\text{cm}^{-1}$ (KBr): 1605m, 1580m, 1525m, 1488m, 1452m, 1385w, 1354w, 1333w, 1300w, 1245w, 1202w, 1164w, 1120w, 1096w, 1031w, 1011w, 984w, 948w, 842s, 788m, 743m, 699w, 657w, 558m, 493w, 469w. m/z 616.2567 [M-PF₆-tol]⁺ calc. for C₃₅H₄₄N₄O₂Zn 616.2756.

2. Crystal images

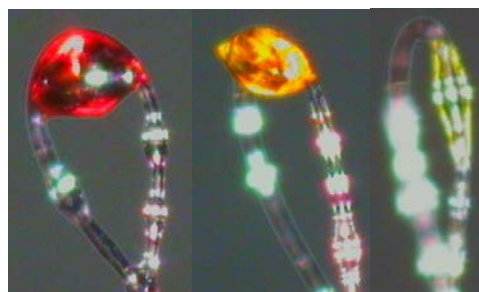


Fig. S1. Crystal images of **1**, **1-Coo.05** and **1-Zn**

3. Thermogravimetric analysis

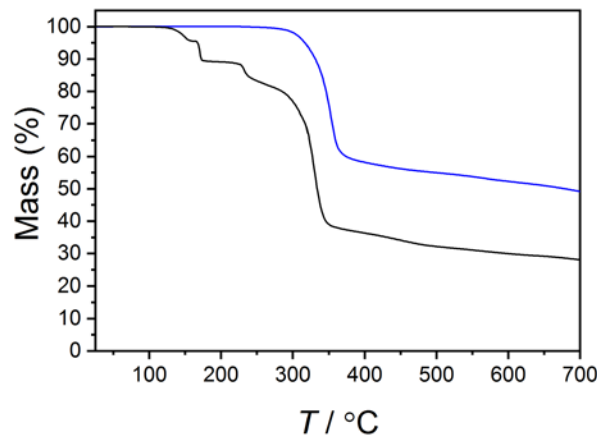


Fig. S2. Thermogravimetric analysis of **2(PF₆)** (blue) and **3(PF₆)·tol** (black)

4. Infrared spectroscopy

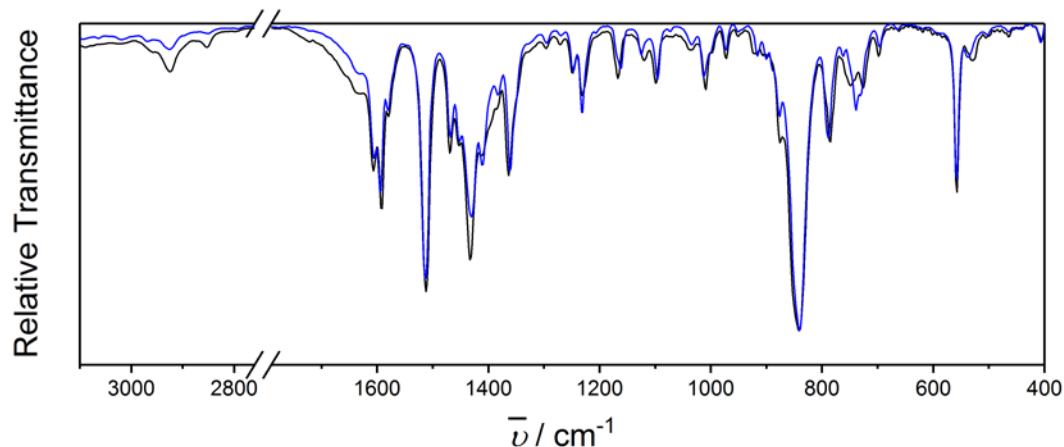


Fig. S3. Infrared spectra of **2(PF₆)** (black) and **2-Zn(PF₆)** (blue)

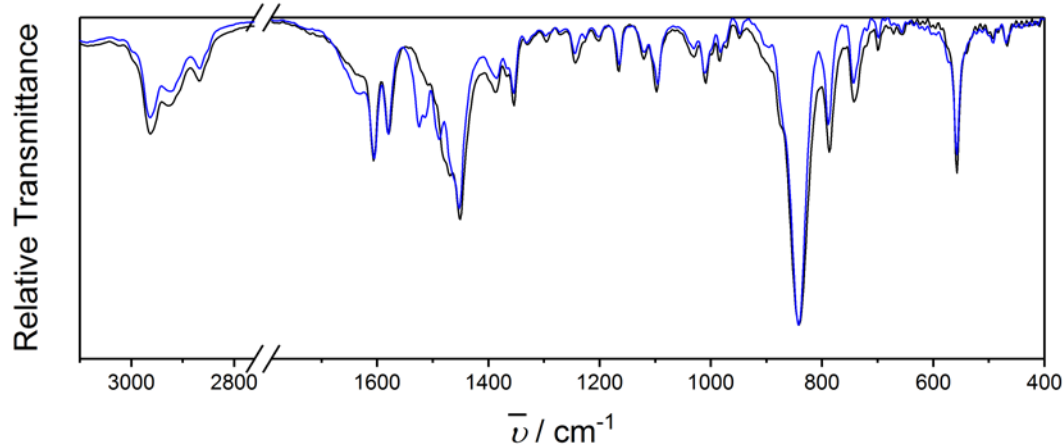


Fig. S4. Infrared spectra of **3(PF₆)·tol** (black) and **3-Zn(PF₆)·tol** (blue)

5. Crystallographic study

5a. Further refinement details

The two independent cobalt complexes in **2(PF₆)**-II are referred to as **2⁺-IIA** and **2⁺-IIB** in the ESI. In **2(PF₆)**-II, **3(PF₆)**·tol and **3-Zn(PF₆)**·tol, the PF₆⁻ anions were found to be disordered, and were constrained to ideal geometry, each distributed over two or three different orientations. For each anion the components of the P atom were constrained to have the same anisotropic displacement parameters (ADP), as were the apical F atoms. The equatorial F atoms were restrained to have similar ADP values. In **3-Zn(PF₆)**·tol, the disordered PF₆⁻ anion showed residual electron density peaks, indicating that the anion was disordered over more than two components; however, attempts to model three components were unsuccessful. There was also evidence of minor disorder in one *tert*-butyl group of one of the crystallographically independent molecules (**3⁺-B**) in **3(PF₆)**·tol and **3-Zn(PF₆)**·tol, and in one toluene molecule and in the PF₆⁻ anion in **2-Zn(PF₆)**·1.5tol-III. However, attempts to model the disorder in **3-Zn(PF₆)**·tol and **2-Zn(PF₆)**·1.5tol-III were unsuccessful as the amount of disorder was too small. Disorder of the *tert*-butyl group of molecule **B** in **3(PF₆)**·tol was able to be modeled over two orientations, with the two components of equivalent carbon atoms restrained to have similar displacement parameters. The toluene molecules in the compounds **2(PF₆)**·1.5tol-III, **2-Zn(PF₆)**·1.5tol-III and **2(PF₆)**·tol-IV were also found to be disordered over two or three positions; for all structures the geometry of each component was constrained to ideal geometry.

5b. Crystallographic data

Table S1. Crystallographic data for compounds **2(PF₆)·II**, **2(PF₆)·1.5tol-III**, **2(PF₆)·tol-IV** and **2-Zn(PF₆)·1.5tol-III**

	2(PF₆)·II	2(PF₆)·1.5tol-III	2(PF₆)·tol-IV	2-Zn(PF₆)·1.5tol-III
formula	C ₂₈ H ₂₉ CoN ₄ O ₂ PF ₆	C _{38.5} H ₄₁ CoN ₄ O ₂ PF ₆	C ₃₅ H ₃₇ CoN ₄ O ₂ PF ₆	C _{38.5} H ₄₁ ZnN ₄ O ₂ PF ₆
fw/g mol ⁻¹	657.45	795.65	749.58	802.09
cryst syst	triclinic	monoclinic	monoclinic	monoclinic
space group	<i>P</i> 1̄	<i>P</i> 2 ₁ /c	<i>P</i> 2 ₁	<i>P</i> 2 ₁ /c
color	red-orange	red-orange	red-orange	pale yellow
<i>a</i> /Å	13.2750(4)	15.4478(4)	9.7975(2)	15.5155(7)
<i>b</i> /Å	13.4480(5)	13.2858(3)	13.6880(2)	13.3294(5)
<i>c</i> /Å	16.9694(5)	18.4890(5)	13.4124(3)	18.3984(8)
α /deg	86.195(3)	90	90	90
β /deg	72.635(3)	103.839(3)	108.897(2)	103.643(5)
γ /deg	84.222(3)	90	90	90
<i>V</i> /Å ³	2874.56(18)	3684.46(17)	1701.77(6)	3697.7(3)
<i>Z</i>	4	4	2	4
<i>T</i> /K	130.00(10)	130.01(10)	130.01(10)	130.01(10)
ρ_{calc} /cm ³	1.519	1.434	1.463	1.441
μ /mm ⁻¹	5.859	4.674	5.023	1.941
reflns measd	21096	15359	14355	28079
unique reflns	11562	7246	6693	7737
data/restraints/param	11562/369/951	7246/0/539	6693/86/542	7737/30/486
<i>R</i> _{int}	0.0261	0.0398	0.0257	0.0635
<i>R</i> _I [<i>I</i> > 2σ(<i>I</i>)]	0.0403	0.0472	0.0291	0.0516
w <i>R</i> ₂ (all data)	0.1120	0.1270	0.0771	0.1501
GOF on F ²	1.036	1.052	1.037	1.035
$\Delta\rho_{max/min}$ /e Å ⁻³	1.19/-0.47	0.61/-0.45	0.19/-0.19	1.19/-0.92

5c. Comparison of **2⁺** in different phases

Table S2. Selected interatomic and intramolecular distances, angles and distortion parameters for complex **2⁺** in each phase

	2(PF₆)-I^a	2(PF₆)-II	2(PF₆)-II	2(PF₆)·1.5tol-III	2(PF₆)·tol-IV
	2⁺-IIA		2⁺-IIB		
<i>Intramolecular and Interatomic Distances and Angles</i>					
Co-O1/Å	2.024(1)	2.015(2)	1.996(2)	1.996(2)	2.002(2)
Co-O2/Å	2.077(1)	2.067(2)	2.087(1)	2.091(2)	2.089(2)
Co-N1/Å	2.127(1)	2.120(2)	2.114(2)	2.114(2)	2.127(2)
Co-N2/Å	2.167(1)	2.181(2)	2.169(2)	2.196(2)	2.179(2)
Co-N3/Å	2.233(1)	2.210(2)	2.210(2)	2.193(2)	2.211(2)
Co-N4/Å	2.242(1)	2.246(2)	2.290(2)	2.300(2)	2.216(2)
C1-O1/Å	1.285(2)	1.293(3)	1.284(3)	1.295(3)	1.281(3)
C2-O2/Å	1.276(2)	1.269(3)	1.278(3)	1.285(3)	1.276(3)
C1-C2/Å	1.480(2)	1.472(4)	1.470(3)	1.474(4)	1.479(4)
O1-Co-O2/deg	78.07(4)	78.40(7)	78.40(6)	78.68(7)	78.31(7)
Co···Co/Å ^b	7.8765(6)		8.2625(6)	8.2688(6)	7.9501(6)
<i>Distortion Parameters</i>					
SHAPE (O _h) ^c	1.715	1.767	1.662	1.733	1.509
Σ/deg ^d	101.7	101.1	97.9	104.9	96.0
Θ/deg ^e	173.6	175.3	178.5	181.9	164.3

^a The bulk sample was phase I and is referred to as **2(PF₆)** in the main text.

^b Minimum intramolecular Co···Co distance.

^c SHAPE index for octahedral geometry, calculated in SHAPE 2.1.^{5,6}

^d Σ = Σ_{i=1}¹²|90 - α_i| where α_i are the twelve cis-O/N-Co-O/N angles about the cobalt atom.⁷

^e Θ = Σ_{j=1}²⁴|60 - θ_j| where θ_j are the 24 unique O/N-C_a-C_b-O/N dihedral angles, |θ_j| < 120°. C_a and C_b are the centroids of two triangular faces that are opposite on the octahedron such that C_a-C_b represents their common pseudo-threefold axis.⁷

5d. Overlaid complex diagrams

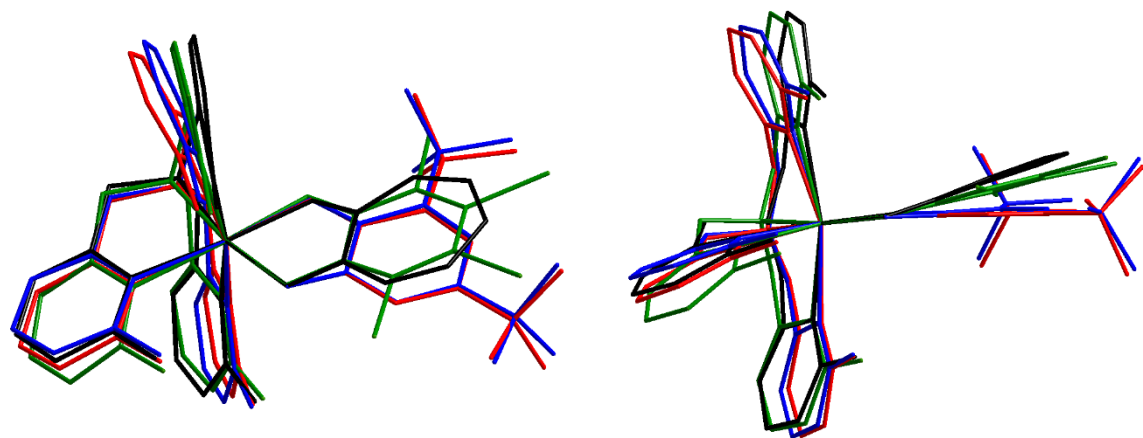


Fig. S5. Overlaid complexes **1** (green), **2⁺-I** (black), **3⁺-A** (blue) and **3⁺-B** (red) viewed from two angles.

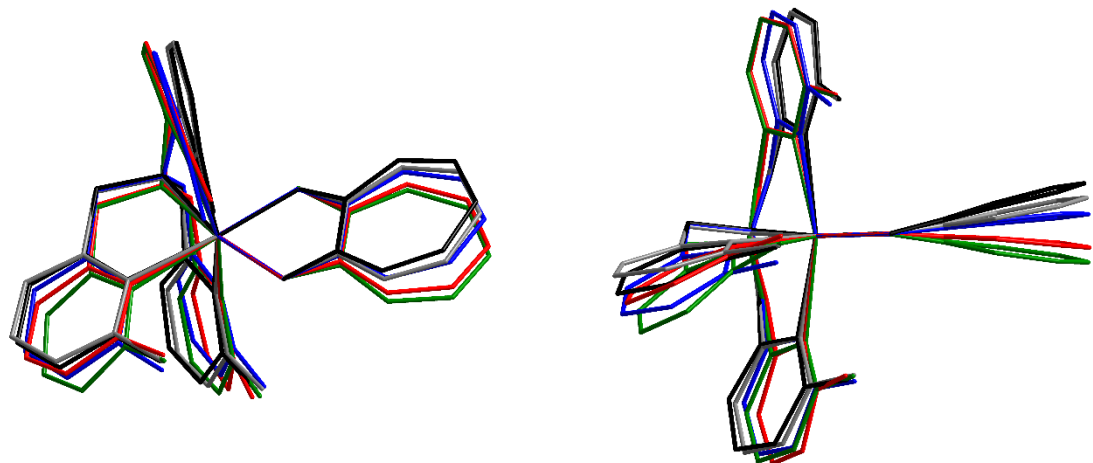


Fig. S6. Overlaid complexes **2⁺-I** (black), **2⁺-IIA** (blue), **2⁺-IIB** (red), **2⁺-III** (green) and **2⁺-IV** (gray) viewed from two angles.

5e. Crystal packing diagrams

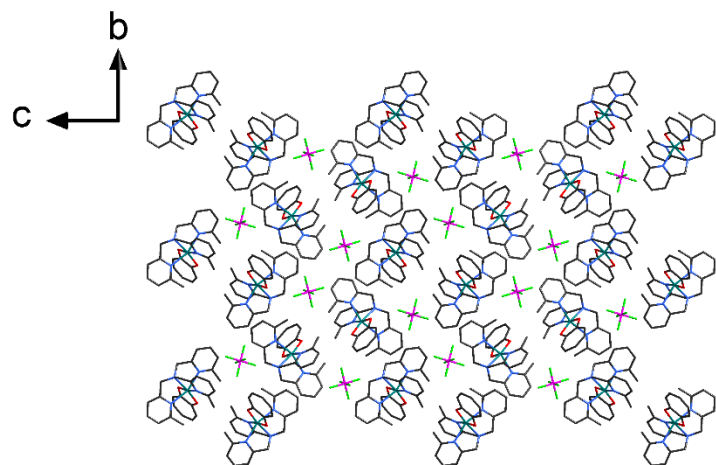


Fig. S7. Crystal packing of **2(PF₆)**-I as viewed along the *a*-axis. Color code: carbon, black; oxygen, red; nitrogen, blue; cobalt, aqua green; phosphorus, magenta; fluorine, bright green.

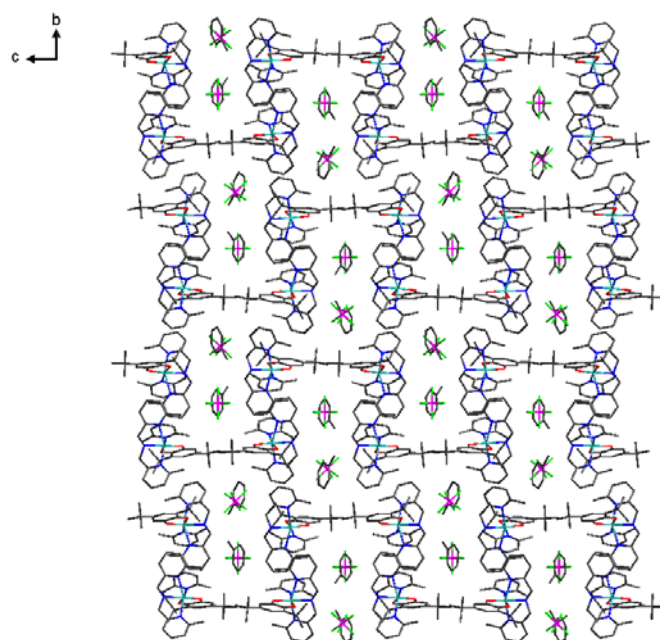


Fig. S8. Crystal packing of **3(PF₆)**·tol as viewed along the *a*-axis. Color code: carbon, black; oxygen, red; nitrogen, blue; cobalt, aqua green; phosphorus, magenta; fluorine, bright green.
Compound **3-Zn(PF₆)**·tol shows identical packing.

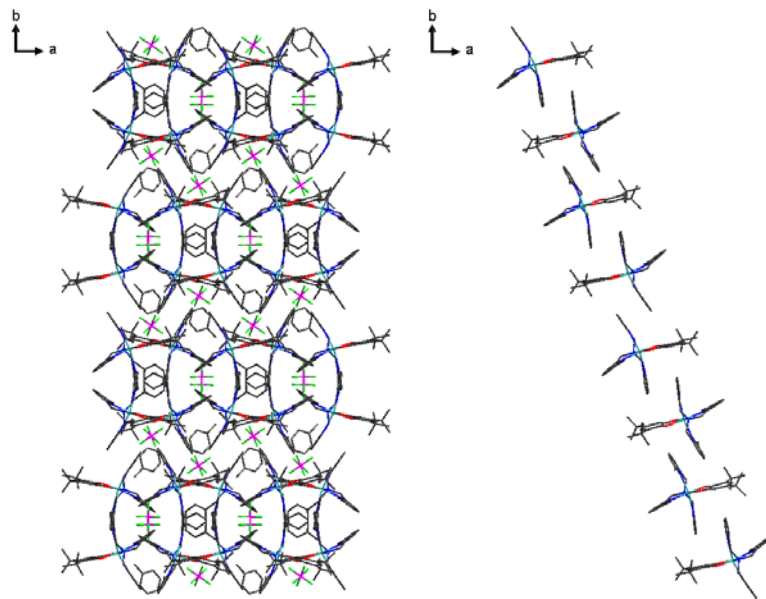


Fig. S9. Crystal packing of **3(PF₆)·tol** as viewed along the *c*-axis (left) and showing selected molecules only (right). Color code: carbon, black; oxygen, red; nitrogen, blue; cobalt, aqua green; phosphorus, magenta; fluorine, bright green. Compound **3-Zn(PF₆)·tol** shows identical packing.

5f. Intermolecular structural parameters in **3(PF₆)·tol**

Table S3. Structural parameters for chain of molecules in **3(PF₆)·tol** and **3-Zn(PF₆)·tol**

Interacting molecules	3(PF₆)·tol			3-Zn(PF₆)·tol		
	3⁺-A/3⁺-B	3⁺-A/3⁺-A	3⁺-B/3⁺-B	3-Zn⁺-A/ 3-Zn⁺-B	3-Zn⁺-A/ 3-Zn⁺-A	3-Zn⁺-B/ 3-Zn⁺-B
<i>Slipped π···π interactions</i>						
Centroid···centroid/Å	4.222	4.713 ^a	3.451	4.294	4.728 ^a	3.456
Minimum C···C/Å	3.275(3)	3.630(3) ^a	3.375(3)	3.296(3)	3.663(3) ^a	3.389(3)
<i>Edge-face C-H···π interactions</i>						
Minimum C···C(H)/Å	3.784(3)	3.597(3)	4.218(3) ^b	3.788(3)	3.604(3)	4.220(3) ^b
Minimum C···H(C)/Å	2.883(2)	2.780(2)	3.313(2) ^b	2.893(2)	2.790(2)	3.318(2) ^b
<i>Selected intermolecular distances and angles</i>						
dbsq···dbsq'/deg ^c	4.43(8)	0	0	4.3(3)	0	0
C1-O1···O2' and C2- O2···O1'/deg	88.20(9)- 92.88(9)	97.93(9)- 100.30(9)	103.03(9)- 119.21(9)	88.43(9)- 93.10(9)	98.06(9)- 100.36(9)	103.17(9)- 119.8(1)
O1···O2' and O2···O1'/Å	8.625(2)- 8.753(2)	8.052(2)	9.338(2)	8.660(2)- 8.785(2)	8.010(2)	9.370(2)
M···M	8.9632(8)	8.3580(9)	8.9184(9)	9.0342(8)	8.3653(9)	8.8990(9)
Spin···spin'/Å ^d	8.90	8.37	9.14	-	-	-

' prime indicates atom or plane belongs to the adjacent molecule.

^a Weak slipped π···π interaction.⁸

^b Intermolecular distance is too short to be considered a non-covalent interaction.⁹

^c dbsq indicates plane defined by O1-O2 and C1-C6.

^d Calculated as the pairwise sum of intermolecular distances, weighted by the Mulliken spin densities for pairs of atoms and normalized for the total spin population of each complex. Sum performed over atoms with significant positive spin density in quintet RAS(20,17) calculation (Co, O1-O2, N1-N4, C1-C5: total spin population 4.002(2)).

6. Powder X-ray diffraction

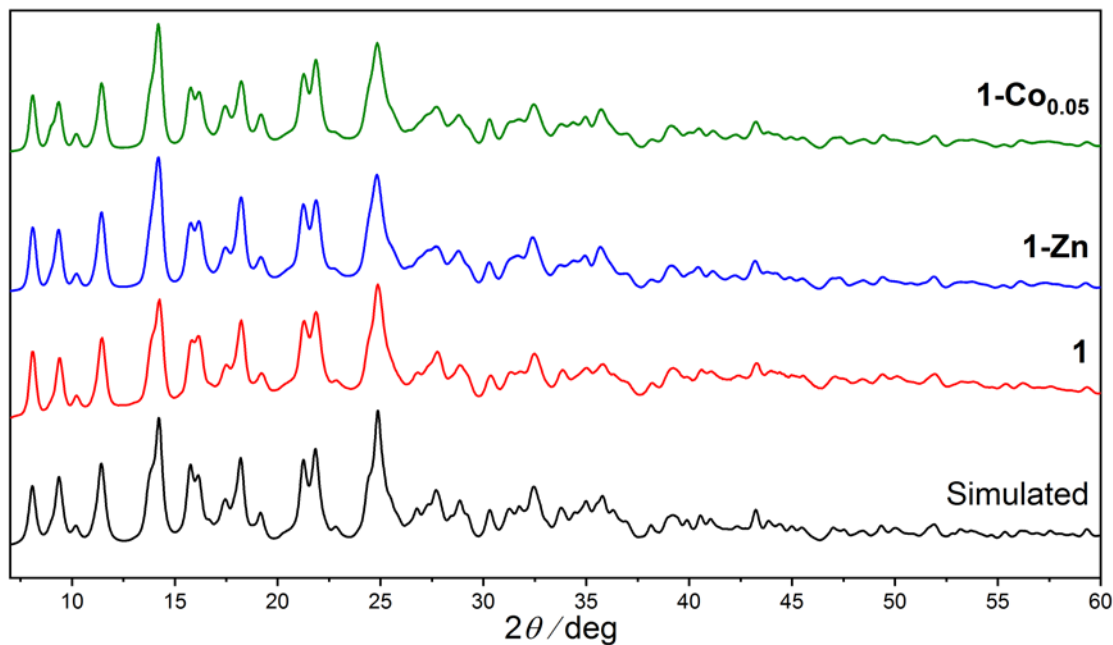


Fig. S10. Simulated powder X-ray diffraction pattern of **1** (black) and experimental pattern of **1** (red), **1-Zn** (blue) and **1-Co_{0.05}** (green).

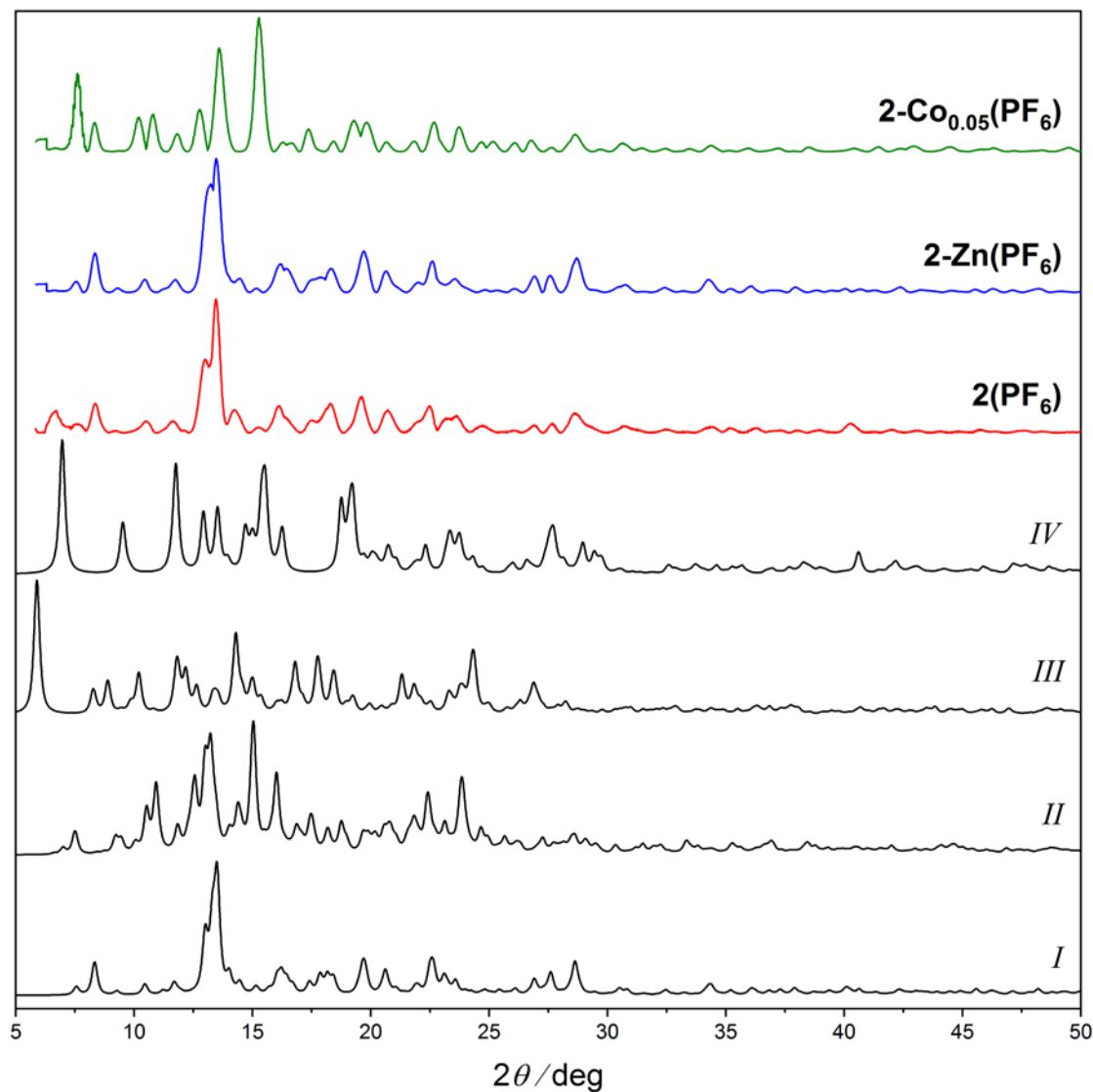


Fig. S11. Simulated powder X-ray diffraction patterns of phases I , II , III and IV of $\mathbf{2}(\text{PF}_6)$ (black) and experimental pattern of bulk sample of $\mathbf{2}(\text{PF}_6)$ (red), $\mathbf{2}\text{-Zn}(\text{PF}_6)$ (blue) and $\mathbf{2}\text{-Co}_{0.05}(\text{PF}_6)$ (green).

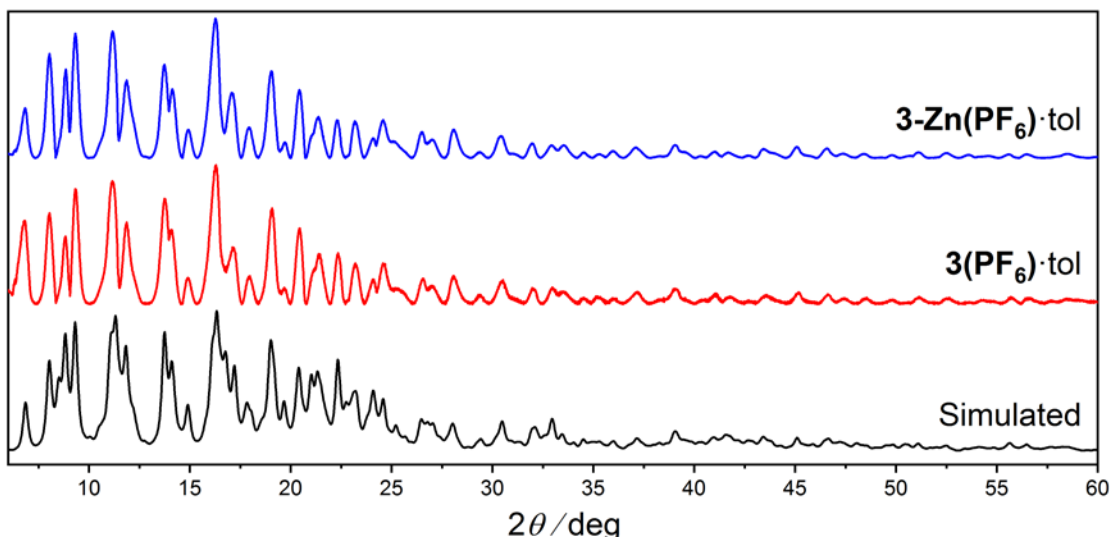


Fig. S12. Simulated powder X-ray diffraction pattern of **3(PF₆)·tol** (black) and experimental pattern of **3(PF₆)·tol** (red) and **3-Zn(PF₆)·tol** (blue).

7. Electronic absorption spectroscopy

Electronic absorption spectra (Fig. S13) in the UV-Vis (220-1000 nm) and near IR (800-1330 nm) were measured for DMF solutions of **1**, **1-Zn**; and acetonitrile solutions of **2(PF₆)**, **2-Zn(PF₆)**, **3(PF₆)** and **3-Zn(PF₆)**. Absorption bands and detailed assignments are presented in Table S4. Compounds **1** and **1-Zn** were measured as DMF solutions due to low solubility in acetonitrile; however, the high absorbance of DMF below 350 nm precluded analysis of the UV range. Data in the visible-range has been reported previously for **1** and **1-Zn** in DMF and **3(PF₆)** in acetonitrile.^{1,4} Mass-spectrometry studies indicate that complexes **2⁺**, **2-Zn⁺**, **3⁺** and **3-Zn⁺** are stable in acetonitrile solution.

The Co complexes exhibit more transitions in the vis-NIR range and are more intensely colored than the Zn analogues. Comparison of the Co and Zn spectra reveals ligand-centered transitions common to both spectra, such as high intensity UV bands and the dbsq-centered transitions around 700-900 nm, and charge transfer and metal-based transitions present only in the Co spectra. The absorption spectra of **2⁺** and **3⁺** are similar to those reported

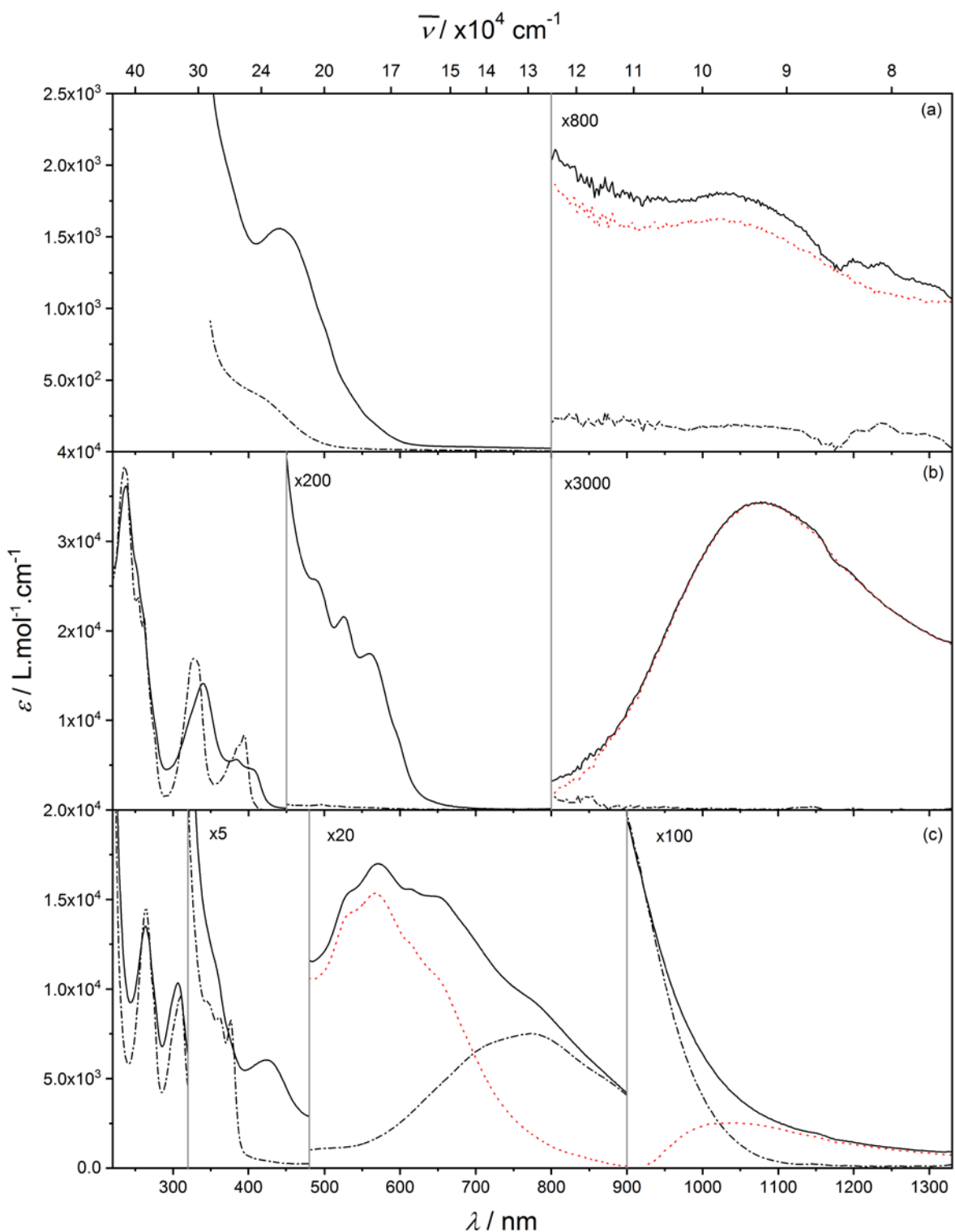


Fig. S13. UV-Vis-NIR absorption spectra of solutions of (a) **1** (black solid) and **1-Zn** (black dashed) in DMF; (b) **2(PF₆)** (black solid) and **2-Zn(PF₆)** (black dashed) in acetonitrile; and (c) **3(PF₆)·tol** (black solid) and **3-Zn(PF₆)·tol** (black dashed) in acetonitrile. Difference spectra between cobalt and zinc complexes are shown in some panels (red dotted).

previously for $[\text{Co}(\text{Me}_4\text{cyclam})(\text{trop})](\text{PF}_6)$ and $\mathbf{3}^+$ respectively, confirming their electronic structure is maintained in solution.^{1,10}

The intense absorption of **1** at 440 nm (DMF) is of similar intensity, position and shape to the absorption band of $\mathbf{3}^+$ at 424 nm (acetonitrile) but similar bands are not observed in the zinc or tropolonate analogues, ruling out the assignment of these bands as ligand-based transitions or $\{\text{Co}(\text{Me}_3\text{tpa})\}$ -based charge transfer transitions. We tentatively assign the 440 nm and 424 nm bands as Co(II)-dioxolene charge transfer transitions.⁴ The absence of the 424 nm absorption band in the spectra of **3-Zn⁺** and the dbsq radical anion,¹¹ confirms that this transition is not semiquinonate-based.

Up to three d-d transitions are expected for octahedral HS-Co(II), corresponding to ${}^4\text{T}_2({}^4\text{F}) \leftarrow {}^4\text{T}_1({}^4\text{F})$, ${}^4\text{A}_2({}^4\text{F}) \leftarrow {}^4\text{T}_1({}^4\text{F})$ and ${}^4\text{T}_1({}^4\text{P}) \leftarrow {}^4\text{T}_1({}^4\text{F})$. The d-d transitions are clearly resolved in **2⁺** as the large separation of the tropolonate π orbitals results in no obscuring visible or NIR bands. The ${}^4\text{T}_1({}^4\text{P}) \leftarrow {}^4\text{T}_1({}^4\text{F})$ transition is clearly split into three bands by the low-symmetry environment, confirming *pseudo*-octahedral geometry.

In **1** and $\mathbf{3}^+$, ligand-centered and charge transfer transitions make the assignment of Co d-d transitions more ambiguous, and they are tentatively assigned based on derivative spectra and the difference spectra with Zn (Fig. S13, Table S4).⁴ The ${}^4\text{A}_2({}^4\text{F}) \leftarrow {}^4\text{T}_1({}^4\text{F})$ transition is not observed in **1**, consistent with its lower intensity,¹² while the peak in the NIR difference spectra of $\mathbf{3}^+$ and **3-Zn⁺** cannot be definitively assigned as ${}^4\text{T}_1({}^4\text{P}) \leftarrow {}^4\text{T}_1({}^4\text{F})$ over a broader dbsq-based absorption band. The assignment of the d-d transitions in **1** and $\mathbf{3}^+$ are not sufficiently reliable to compare the ligand field splitting with **2⁺**; however, they can confirm *pseudo*-octahedral geometry.

Table S4. Electronic Absorption Bands for Compounds **1**, **1-Zn**, **2(PF₆)**, **2-Zn(PF₆)**, **3(PF₆)** and **3-Zn(PF₆)**.

Assignment ^a		λ/nm	$\bar{\nu} / \text{cm}^{-1}$	($\varepsilon/\text{L}\cdot\text{mol}^{-1}\cdot\text{cm}^{-1}$)		λ/nm	$\bar{\nu} / \text{cm}^{-1}$	($\varepsilon/\text{L}\cdot\text{mol}^{-1}\cdot\text{cm}^{-1}$)
1								
LC		377	2.65×10^4	$(1.88 \times 10^3\text{sh})$		408	2.45×10^4	(409sh)
CT		440	2.27×10^4	(1.56×10^3)				
${}^4\text{T}_1(\text{P}) \leftarrow {}^4\text{T}_1(\text{F})$		497	2.01×10^4	(915sh)				
			543^b	1.84×10^4	(336sh)			
			567^b	1.76×10^4	(194sh)			
${}^4\text{T}_2({}^4\text{F}) \leftarrow {}^4\text{T}_1({}^4\text{F})$		1027	9.74×10^3	(22sh)				
2⁺								
LC (trop) $\pi \rightarrow \pi^*$ ^c						233 ^b	4.29×10^4	$(3.72 \times 10^4\text{sh})$
		238	4.20×10^4	(3.62×10^4)		236	4.24×10^4	(3.83×10^4)
						238	4.20×10^4	$(3.79 \times 10^4\text{sh})$
						244	4.10×10^4	$(3.00 \times 10^4\text{sh})$
		251		$(2.76 \times 10^4\text{sh})$		253	3.95×10^4	(2.39×10^4)
		258		$(2.31 \times 10^4\text{sh})$		262	3.82×10^4	(2.14×10^4)
		277		$(9.11 \times 10^3\text{sh})$		274	3.65×10^4	(9.20×10^3)
						311 ^b	3.22×10^4	$(7.62 \times 10^3\text{sh})$
		325 ^b		$(1.09 \times 10^4\text{sh})$		327	3.06×10^4	(1.69×10^4)
		340	2.94×10^4	(1.41×10^4)		330 ^b	3.03×10^4	(1.68×10^4)
						357 ^b	2.80×10^4	$(2.92 \times 10^3\text{sh})$
						365 ^b	2.74×10^4	$(3.54 \times 10^3\text{sh})$
						377	2.65×10^4	$(5.61 \times 10^3\text{sh})$
		383	2.61×10^4	(5.61×10^3)		387	2.58×10^4	$(7.20 \times 10^3\text{sh})$
		401	2.49×10^4	$(4.66 \times 10^3\text{sh})$		394	2.54×10^4	(8.34×10^3)
${}^4\text{T}_1(\text{P}) \leftarrow {}^4\text{T}_1(\text{F})$		485	2.06×10^4	(129sh)				
		526	1.90×10^4	(108)				

	560	1.79×10^4	(87)			
${}^4\text{A}_2(\text{F}) \leftarrow {}^4\text{T}_1(\text{F})$	595	1.68×10^4	(43sh)			
${}^4\text{T}_2({}^4\text{F}) \leftarrow {}^4\text{T}_1({}^4\text{F})$	1077	9.29×10^3	(11)			
	3⁺			3-Zn⁺		
LC (dbsq) ^d	264	3.79×10^4	(1.35×10^4)	264	3.78×10^4	(1.46×10^4)
	275 ^b	3.64×10^4	(9.90×10^3 sh)	274	3.65×10^4	(9.71×10^3 sh)
	298 ^b	3.36×10^4	(9.15×10^3 sh)	302 ^b	3.31×10^4	(8.19×10^3 sh)
	306	3.27×10^4	(1.03×10^3)	310	3.23×10^4	(9.64×10^3)
	354 ^e	2.82×10^4	(2.36×10^3 sh)	346 ^e	2.89×10^4	(1.87×10^3)
				362 ^e	2.76×10^4	(1.68×10^3)
	375 ^b	2.67×10^4	(1.47×10^3 sh)	376 ^e	2.66×10^4	(1.66×10^3)
CT	424	2.36×10^4	(1.21×10^3)			
unassigned	493 ^b	2.03×10^4	(590sh)	427	2.34×10^4	(79sh)
				510	1.96×10^4	(59sh)
${}^4\text{T}_1(\text{P}) \leftarrow {}^4\text{T}_1(\text{F})^f$	537	1.86×10^4	(773sh)			
	610	1.64×10^4	(779sh)			
	642	1.56×10^4	(759sh)			
MLCT ^f	571	1.75×10^4	(850)			
LC (dbsq) ^d				729	1.37×10^4	(354sh)
	769	1.30×10^4	(477sh)	771	1.30×10^4	(375)
	866	1.15×10^4	(274sh)	869	1.15×10^4	(253sh)
${}^4\text{T}_2({}^4\text{F}) \leftarrow {}^4\text{T}_1({}^4\text{F})^g$	1037	9.64×10^3	(43sh)			

^a LC = ligand-centered, CT = charge transfer, MLCT = metal-to-ligand charge transfer.

^b Bands can only be distinguished in derivative spectrum.

^c Assignments are based on V and Cu complexes with tropolonate.^{13,14}

^d Assignments based on transitions observed for dbsq⁻.¹¹

^e Vibronic structure only observed in **3-Zn⁺**.

^f All bands were previously assigned as MLCTs between the Co(II) d-orbitals and dbsq⁻ π*,¹ assignment as MLCT or d-d transition is tentative.

^g Assigned based on (**3⁺**) – (**3-Zn⁺**) difference spectrum as d-d transition is obscured by LC (dbsq) band.

8. EPR spectroscopy

8a. EPR of **1** and **2(PF₆)**

Table S5. EPR simulation parameters, optimized for X-band **1-COO.05** and W-band **2(PF₆)**

	<i>1</i>	<i>2</i>	<i>3</i>
1-COO.05 / 1			
<i>g</i> -values	5.815	3.975	2.19
<i>g</i> -strain / MHz	0.18	0.085	0.025
<i>A</i> -values / MHz	570	210	175
<i>H</i> -strain / MHz ^a	700	900	500
2(PF₆)			
<i>g</i> -values	5.579	3.872	3.118
<i>g</i> -strain / MHz	0.3	0.19	0.18
<i>A</i> -values / MHz	470	325	262
<i>H</i> -strain / MHz	900	900	900

^a *H*-strain was used in the simulation of **1** but was not required for **1-COO.05**

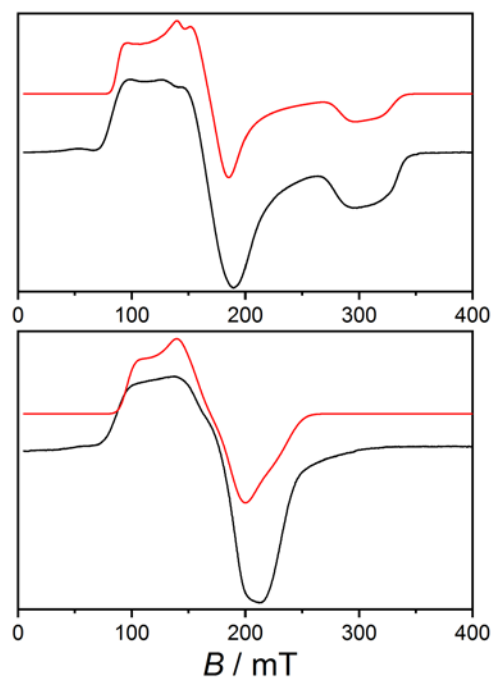


Fig. S14. Solid state X-band EPR spectra at 10 K of (top) **1** and (bottom) **2(PF₆)** (black) with simulations (red). Simulation parameters are indicated in Table S5.

8b. EPR of **3-Zn(PF₆)·tol**

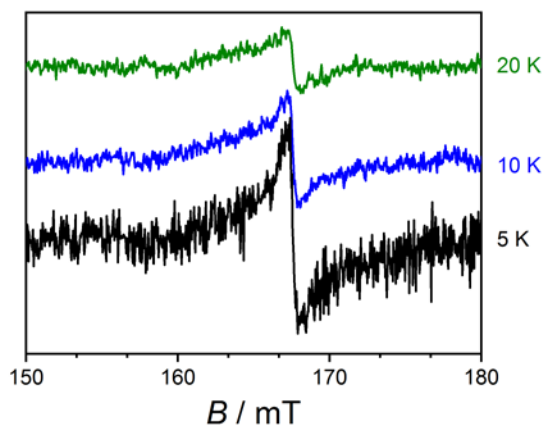


Fig. S15. EPR half-field transition in **3-Zn(PF₆)·tol**

9. Magnetic data

9a. Static magnetic data for **3(PF₆)·tol** restrained in eicosane compared to PTFE pellet

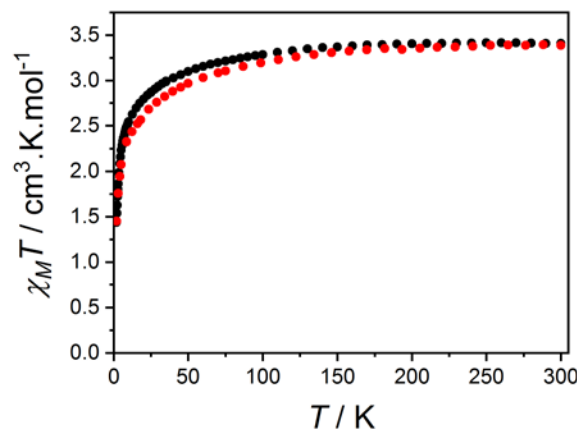


Fig. S16. Plot of $\chi_M T$ versus T for **3(PF₆)·tol** restrained in a PTFE pellet (black) or restrained in eicosane (red).

9b. Chain model of **3-Zn(PF₆)·tol**

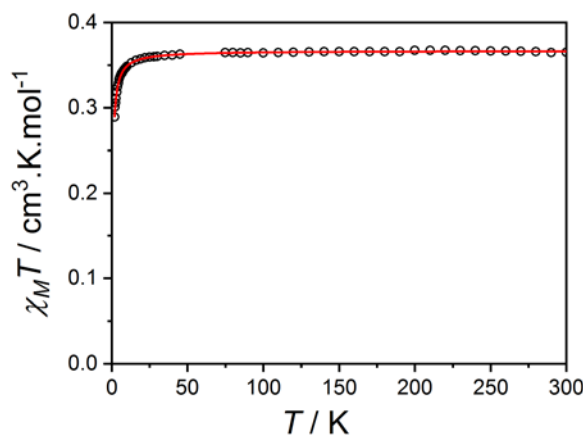


Fig. S17. Low temperature plot of $\chi_M T$ versus T per mole of **3-Zn(PF₆)·tol** monomer (black circles), showing fit to the Bonner Fisher approximation¹⁵ (red line) with $J = -0.386(2) \text{ cm}^{-1}$ and $g = 1.978(3)$.

9c. Curie-Weiss plot of **3-Zn(PF₆)·tol**

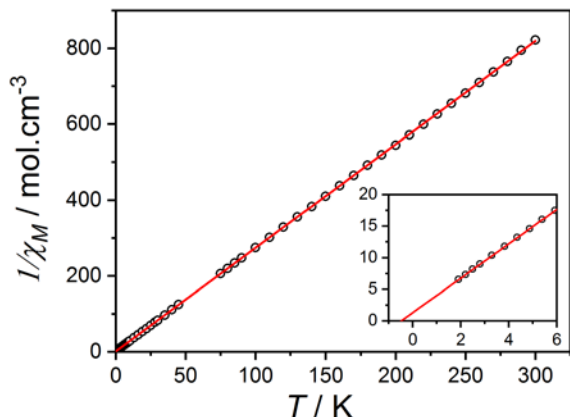


Fig. S18. Curie-Weiss plot for two molecules of **3-Zn(PF₆)·tol** with overlaid fit to the Curie-Weiss law: Curie constant = $0.3667 \pm 0.0002 \text{ cm}^3 \text{ K mol}^{-1}$ and Weiss constant = $-0.48 \pm 0.06 \text{ K}$. Inset: close-up of low-temperature region.

9d. Dynamic magnetic data for **3(PF₆)·tol**

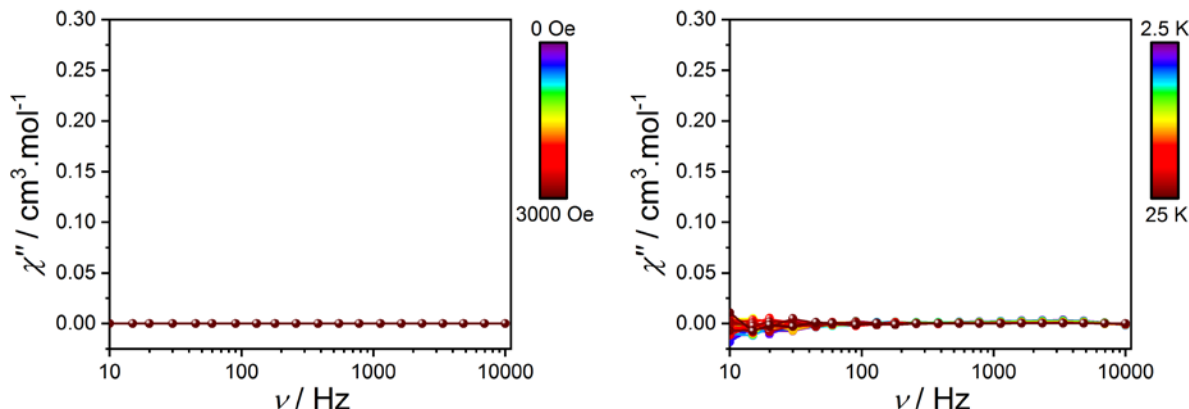


Fig. S19. The absence of an out-of-phase magnetic susceptibility (solid circles) for **3(PF₆)·tol** showing frequency-dependence at different fields at 2.5 K (left) and temperature-dependence under an applied field of 0 T (right). Vertical scale is the same as for **1** in Fig. 11. Lines are guides for the eye.

10 Inelastic neutron scattering

10a. Supplementary figures for 3(PF₆)·tol INS with 4.69 Å neutrons

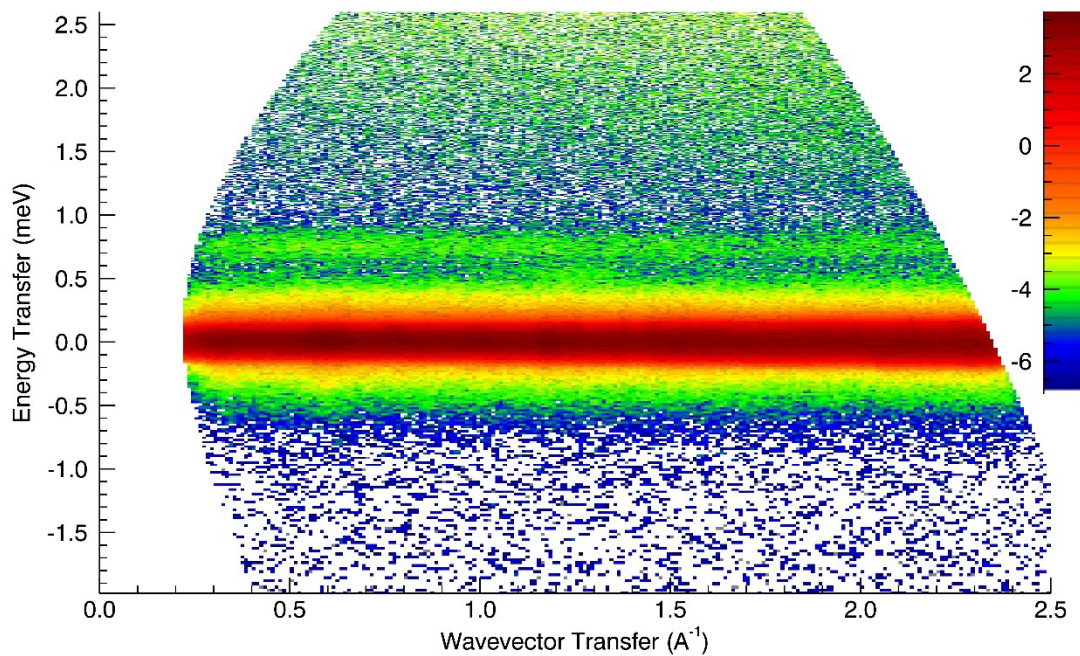


Fig. S20. Plot of $S(Q,E)$ for 3(PF₆)·tol at 1.5 K. Color scale indicates the order of magnitude of the intensity. Note that 1 meV \approx 8.066 cm⁻¹.

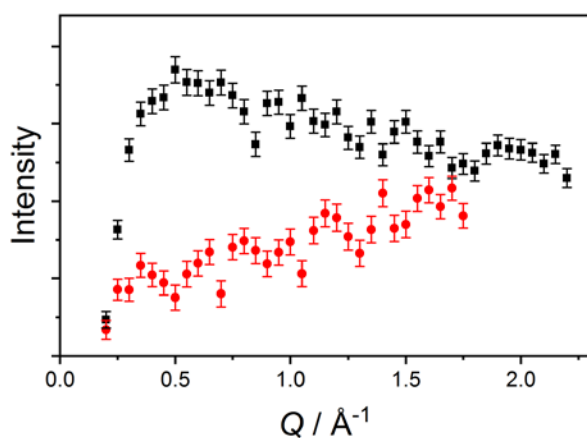


Fig. S21. Q -dependence of transitions integrated at 6.0(1.6) cm⁻¹ (black squares) and 14.5(1.6) cm⁻¹ (red circles) for 3(PF₆)·tol at 1.5 K.

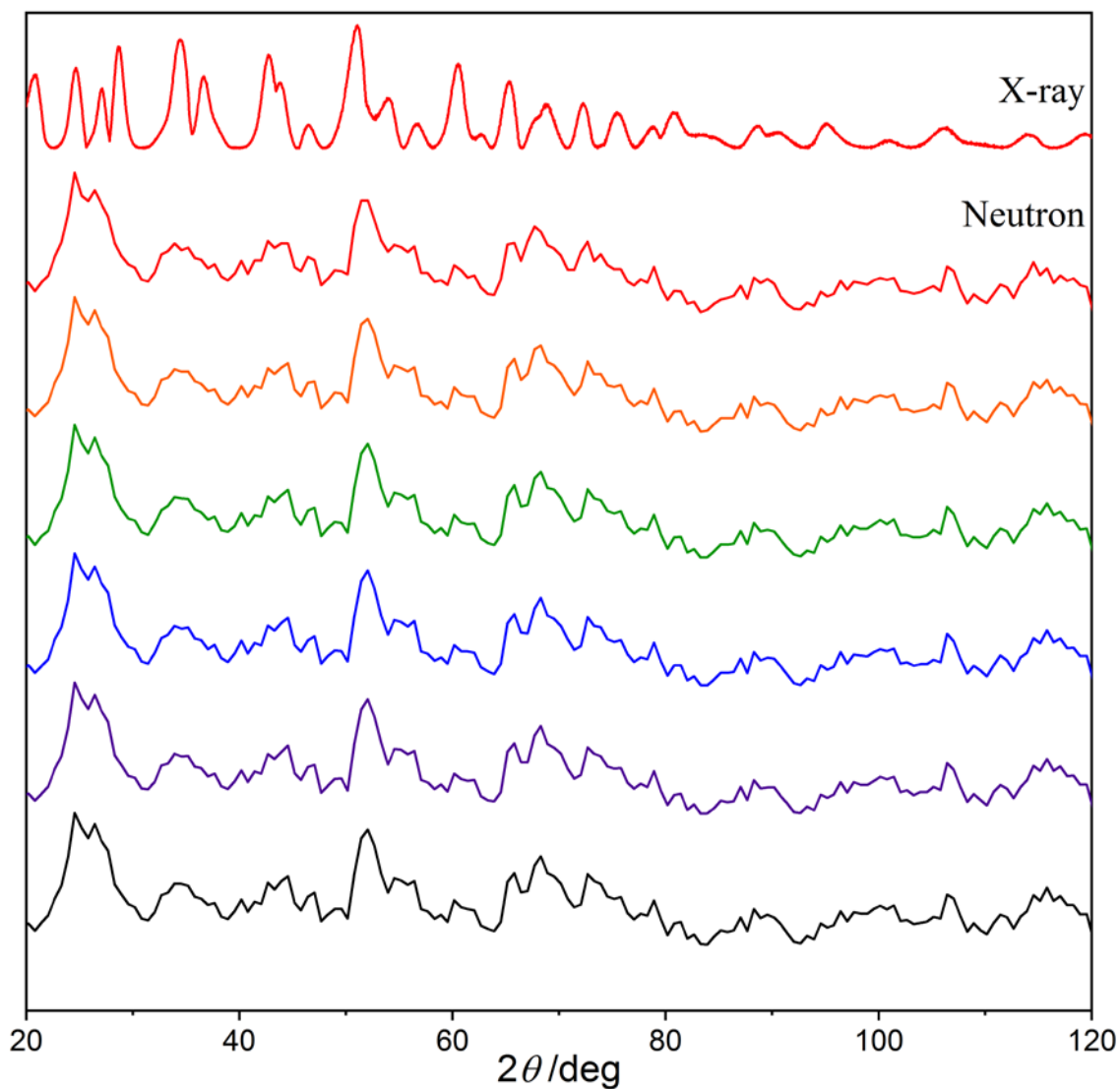


Fig. S22. Variable temperature powder diffraction patterns of $\mathbf{3}(\text{PF}_6)\cdot\text{tol}$ with neutrons at 1.5 K (black), 5 K (purple), 10 K (blue), 25 K (green), 50 K (orange) and 100 K (red). Experimental X-ray powder diffraction pattern at 100 K (red) corrected for the different wavelength used.

Table S6. Predicted INS transitions for **3(PF₆)·tol** from individual molecule *ab initio* RASSCF/RASSI-SO calculations

	Hot/Cold	Energy / cm ⁻¹	Relative intensity
3⁺-A			
$ 1_A\rangle \rightarrow 2_A\rangle$	Cold	6.59	5.40
$ 1_A\rangle \rightarrow 3_A\rangle$	Cold	55.0	2.55
$ 1_A\rangle \rightarrow 4_A\rangle$	Cold	63.3	0.57
$ 2_A\rangle \rightarrow 3_A\rangle$	Hot	48.4	2.33
$ 2_A\rangle \rightarrow 4_A\rangle$	Hot	56.7	0.10
3⁺-B			
$ 1_B\rangle \rightarrow 2_B\rangle$	Cold	5.70	4.74
$ 1_B\rangle \rightarrow 3_B\rangle$	Cold	33.14	0.69
$ 1_B\rangle \rightarrow 4_B\rangle$	Cold	54.14	2.37
$ 2_B\rangle \rightarrow 3_B\rangle$	Hot	27.44	0.53
$ 2_B\rangle \rightarrow 4_B\rangle$	Hot	48.44	2.04

10b. Further INS measurements

Inelastic neutron scattering data were also collected for **3-Zn(PF₆)·tol**, as a radical-only isomorphous analogue of **3(PF₆)·tol**, to aid in the identification of phonon bands. On the basis of its magnetic susceptibility, compound **3-Zn(PF₆)·tol** is predicted to display a single magnetic INS transition at $\sim 1\text{ cm}^{-1}$, which is expected to be obscured by the elastic scattering peak. Spectra obtained at 1.5 K and scaled to maximum intensity (Fig. S23) show the same 16 cm^{-1} feature as **3(PF₆)·tol**, confirming that this transition is of phononic origin. The increase in intensity for the 16 cm^{-1} band with increasing Q is further confirmation of a phonon transition (Fig. S24).

Spectra of **3-Zn(PF₆)·tol** show a very weak excitation at $E = 6.3(1)\text{ cm}^{-1}$, of approximately 1/12 of the intensity of the 6.00(8) cm^{-1} peak in **3(PF₆)·tol**. The 6.3(1) cm^{-1} excitation shows a reduction in intensity with increasing temperature (Fig. S23). The relatively low counting statistics of this excitation mean that it is difficult to extract the Q -dependence and to assign the peak. The observed Q -dependence is approximately flat (Fig. S24), showing neither the quadratic dependence of a phonon, nor the exponential decay associated with a magnetic excitation. This peak also lies in very close proximity to both the elastic line, which contains some quasi-elastic signal, and the tail of the phonon. The Q -integral could contain a combination of phononic, magnetic and quasi-elastic scattering to result in a very flat intensity; however, if a magnetic transition does occur as part of the excitation at 6.3(1) cm^{-1} , it is of a different origin to the 6.00(8) cm^{-1} peak, which arises from Co(II)-dbsq intermolecular interactions, as described in the main text.

Data measured with the shorter neutron wavelength of 2.345 Å also reveals a series of peaks for **3(PF₆)·tol** and **3-Zn(PF₆)·tol** (Fig. S25). The common peaks between the two samples as well as the temperature and Q -dependence of these excitations indicate that this higher energy region is dominated by phonon modes, which is unsurprising giving the hydrogenous nature of the sample.

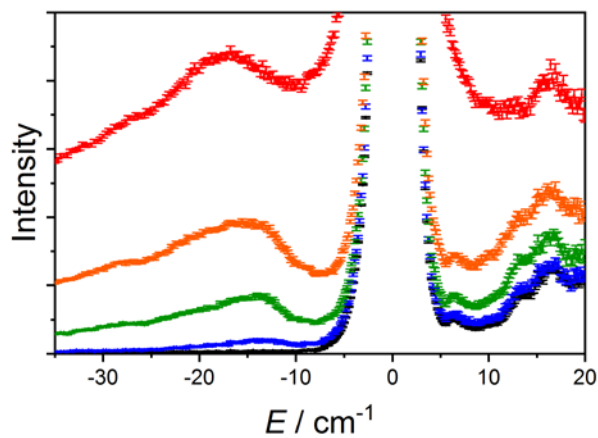


Fig. S23. Temperature dependence of $S(E)$ for **3-Zn(PF₆)·tol** with integration over the whole Q -range. Color code: 1.5 K, black; 10 K, blue; 25 K, green; 50 K, orange; 100 K, red.

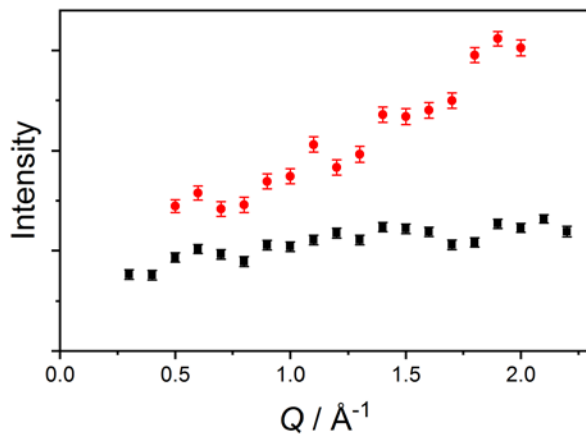


Fig. S24. Q-dependence of transitions integrated at 6.3(1.6) cm^{-1} (black squares) and 14.5(1.6) cm^{-1} (red circles) for **3-Zn(PF₆)·tol** at 1.5 K.

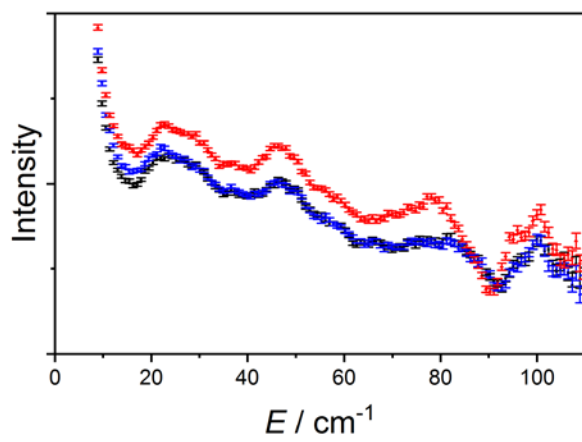


Fig. S25. $S(E)$ for $\mathbf{3}(\text{PF}_6)\cdot\text{tol}$ at 1.5 K (black) and 10 K (blue) and $\mathbf{3}\text{-Zn}(\text{PF}_6)\cdot\text{tol}$ at 1.5 K (red) using $\lambda = 2.345 \text{ \AA}$ neutrons.

11. Theoretical calculations on Co(II) analogues

11a. Discussion of theoretical calculations on Co(II) analogues

Ab initio calculations were performed in order to clarify the Co(II) electronic state in **1** and **2⁺**. Cobalt(II) has a 3d⁷ electronic configuration, resulting in 10 spin quartets and 40 spin doublets and giving a ground state of ⁴T_{1g} in an octahedral crystal field. Previous *ab initio* calculations of *pseudo*-octahedral Co(II) have used a simple complete active space (CAS(7,5)) calculations averaging over all quartets and doublets.¹⁶⁻¹⁸ However, active space selection must be optimized for each molecule individually to reproduce magnetic and spectroscopic data.

Restricted active space (RAS) calculations gave access to a larger active space than was possible with CAS calculations. The best reproduction of magnetic data for **2⁺** was found to be a RAS(19,2,2;4,7,3) (RAS(19,14), Fig. S26) averaged over the three lowest energy spin quartet states, which would make up the ⁴T_{1g} ground state in a strictly octahedral crystal field. Simultaneous consideration of the core Co 3s, 3p orbitals and the double shell Co 4d_π slightly improved the magnetic susceptibility profile when compared to a CAS(7,5) calculation for both **1** and **2⁺**, despite the extreme occupations (> 1.9984 and < 0.0116). The double shell Co 4d_σ orbitals were excluded due to their lesser occupation than the Co 4d_π orbitals when averaging over the three lowest energy spin quartets; the Co 4d_σ became unstable in the active space when competing with Co 4p orbitals correlated to Co 3p. A slight improvement in the reproduction of the experimental magnetic susceptibility was found with the addition of the σ-bonding orbitals for **2⁺**, included in RAS2, as recommended for first row transition metal complexes.¹⁹ The **1** σ-bonding orbitals were not stable in RAS2, were highly occupied (>1.9988) and distorted in RAS1, and did not improve simulation of magnetic or EPR data; σ-bonding orbitals were excluded for **1** to give RAS(15,2,2;4,5,3) (RAS(15,12), see Fig. S26).

Reproduction of the magnetic data and ground state g-values of **2(PF₆)** by RASSCF/RASSI-SO *ab initio* calculations is excellent (Table S5, Table S11). The KD energies from *ab initio* agree well with those derived from fitting the experimental data (Table S9) and

indeed fitting the Griffith model to the *ab initio* data reveals similar parameters with a smaller B_2^2 term than obtained by fitting experimental data: $\alpha = -1.3336(9)$, $B_2^0 = -57.9(6) \text{ cm}^{-1}$ and $|B_2^2| = 38(2) \text{ cm}^{-1}$. *Ab initio* RASSCF/RASSI-SO calculations on the different polymorphs of **2⁺** indicate the anisotropy of the ground state is strongly sensitive to geometry (Table S7 and S9) and the Co(II) electronic structure of **3⁺** cannot be assumed to have the same anisotropy as **2⁺**.

Reproduction of magnetic data of **1** is reasonable and shows poorer agreement between RASSCF/RASSI-SO *ab initio* spin-orbit energies and those derived from fitting the experimental data to the Griffith model, Equation (1) (Table S8). Fitting of the Griffith model to the *ab initio* data in the program PHI indicates the deviation between calculation and experiment is primarily the result of an inverted and reduced B_0^2 term and therefore lesser splitting of the states arising from the orbital quartet: $\alpha = -1.2917(2)$, $B_2^0 = -77.6(2) \text{ cm}^{-1}$ and $|B_2^2| = 74.4(5) \text{ cm}^{-1}$. Reproduction of EPR spectroscopic data of **1** show good agreement for g_1 and g_2 (Table 2) but a variation of 0.5 in the value of g_3 . The large calculated energy gaps between the first and second KD in **1** and **2⁺** ($> 200 \text{ cm}^{-1}$) support the observation of an isolated magnetic ground state.

11b. Spin-only energies of Co(II) analogues

Table S7. *Ab initio* RASSCF spin-only quartet state energies of **1** and **2⁺**

1 / cm⁻¹	2⁺-I / cm⁻¹	2⁺-IIA / cm⁻¹	2⁺-IIB / cm⁻¹	2⁺-III / cm⁻¹	2⁺-IV / cm⁻¹
0	0	0	0	0	0
418.410	108.363	135.529	105.805	84.810	175.64
509.452	327.050	243.427	397.039	513.406	330.56

11c. Spin-orbit energies of Co(II) analogues

Table S8. Simulated spin-orbit quartet KD energies (cm^{-1}) of **1** from *ab initio* RASSCF/RASSI-SO and fitting the Griffith model to experimental data

<i>Ab initio</i>	Griffith
0	0
226.219	139.128
525.629	549.183
922.209	791.801
1041.62	1045.98
1174.83	1128.21

Table S9. Simulated spin-orbit quartet KD energies (cm^{-1}) of polymorphs of **2⁺** from *ab initio* RASSCF/RASSI-SO and fitting the Griffith model to experimental data

<i>Ab initio</i>	<i>Ab initio</i>	<i>Ab initio</i>	<i>Ab initio</i>	<i>Ab initio</i>	Griffith
2⁺-I	2⁺-IIA	2⁺-IIB	2⁺-III	2⁺-IV	2(PF₆)
0	0	0	0	0	0
282.193	291.709	272.329	262.509	272.187	244.511
425.569	405.112	432.624	459.334	433.016	409.372
859.667	861.738	840.797	838.344	860.321	787.409
989.876	951.293	1022.53	1104.65	978.010	947.640
1053.75	1022.17	1092.76	1163.91	1051.39	1004.59

Table S10. Spin-orbit quartet KD energies (cm^{-1}) of **3** from *ab initio* RASSCF/RASSI-SO and fitting the Griffith model to the *ab initio* simulation

<i>Ab initio</i>	Griffith	<i>Ab initio</i>	Griffith
3-A	3-A	3-B	3-B
0	0	0	0
253.267	289.827	294.315	254.088
563.960	495.302	479.475	555.833
977.546	934.355	932.404	941.162
1153.02	1168.55	1087.23	1273.78
1290.46	1236.11	1215.17	1353.56

11d. Theoretical *g*-values and *g*-tensors in Co(II) analogues

Table S11. *Ab initio* RASSCF/RASSI-SO simulated *g*-values of ground KD of **2⁺**

2^{+-I}	2^{+-IIA}	2^{+-IIB}	2^{+-III}	2^{+-IV}
5.646	4.825	5.649	6.376	5.132
3.687	4.372	3.798	3.289	4.282
3.177	3.382	3.022	2.655	3.116

Table S12. *Ab initio* RASSCF/RASSI-SO *g*-values of KDs for **3-A** and values from fitting the Griffith model to the *ab initio* simulation

KD	<i>Ab initio</i>			Griffith		
1	3.0060	3.7316	5.8596	3.0160	3.7200	5.8616
2	0.0767	1.0439	3.7919	0.1392	1.1146	3.8914
3	1.5140	1.8445	2.4957	1.2901	2.1681	2.4911
4	0.1170	0.4280	2.9692	0.0784	0.1023	3.1658
5	0.4888	1.8153	2.1684	0.7034	1.1531	3.6249
6	0.1400	0.1434	2.9555	1.0022	1.2342	3.1899

Table S13. *Ab initio* RASSCF/RASSI-SO *g*-values of KDs for **3-B** and values from fitting the Griffith model to the *ab initio* simulation

KD	<i>Ab initio</i>			Griffith		
1	2.5905	3.6263	6.2107	2.6033	3.6117	6.2139
2	0.8623	1.2180	4.6657	0.7709	1.3541	4.5197
3	1.5893	2.4711	4.0344	1.1051	2.7547	3.5742
4	0.0307	0.8024	2.8622	0.2078	0.2609	3.2102
5	0.3500	1.8839	2.1830	0.7782	1.4520	3.9389
6	0.1101	0.1119	3.0548	0.9740	1.1279	3.3812

11e. Optimized orbitals for Co(II) analogues

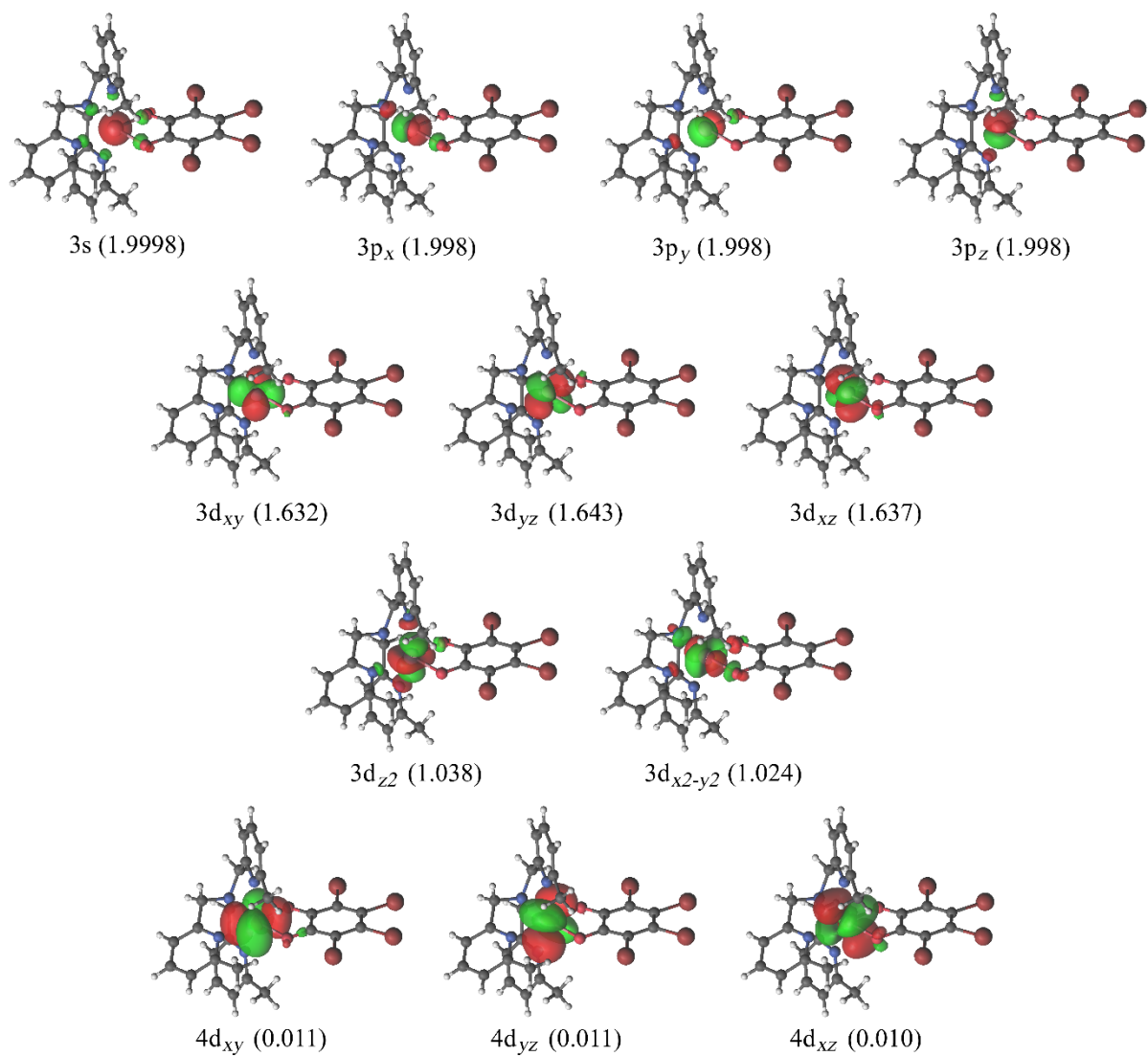


Fig. S26. Active orbitals for $^4\text{T}_1$ state of **1** for the RAS(15,2,2;4,5,3) active space. The contour values are $\pm 0.03 \text{ e/au}^3$. Orbitals are labelled by predominant character and natural occupation numbers are given within parentheses.

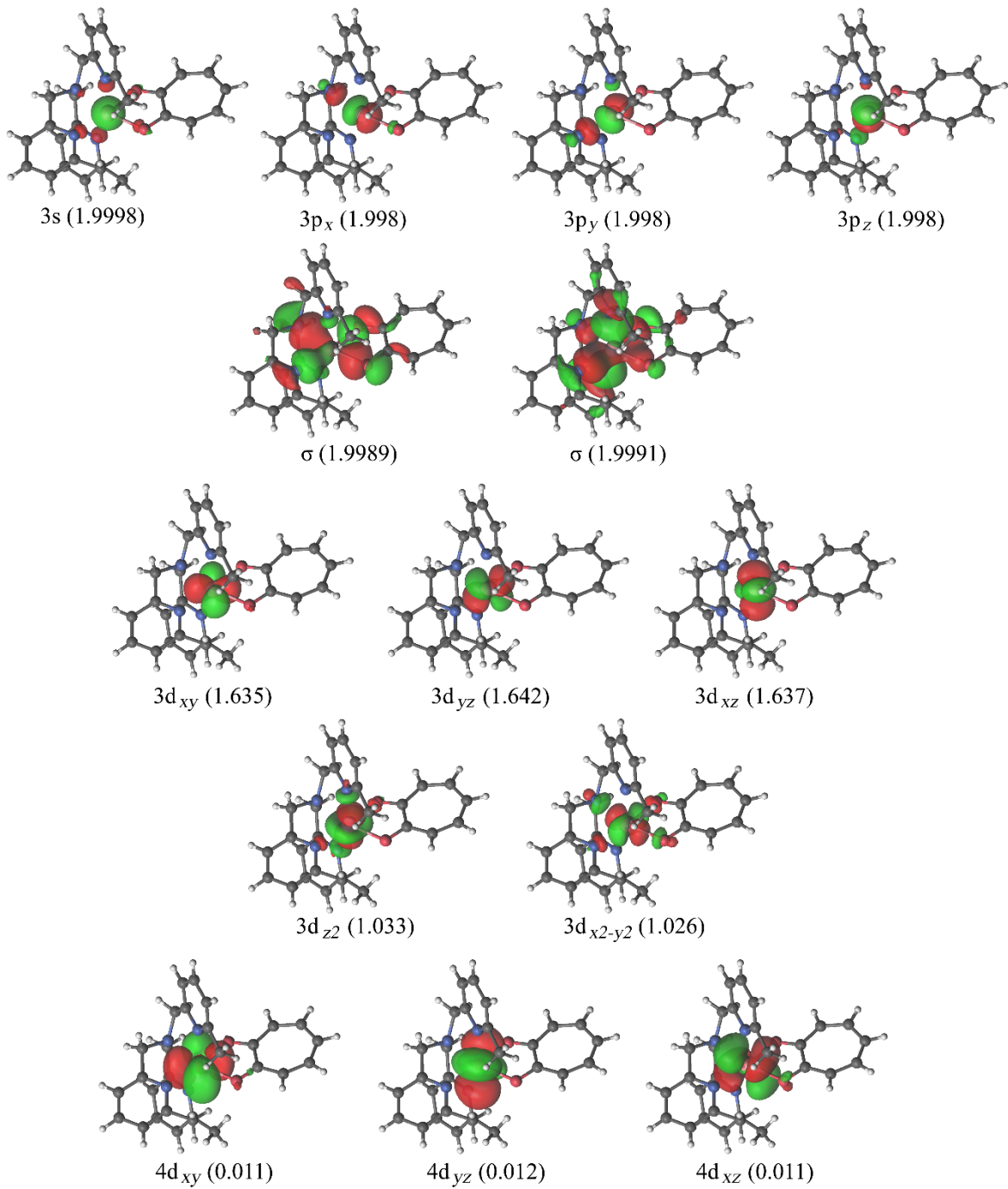


Fig. S27. Active orbitals for ${}^4\text{T}_1$ state of $\mathbf{2}^+\text{-}\text{I}$ for the RAS(19,2,2;4,7,3) active space. The contour values are $\pm 0.03 \text{ e/au}^3$. Orbitals are labelled by predominant character and natural occupation numbers are given within parentheses. Equivalent orbitals are observed for other polymorphs of $\mathbf{2}^+$

12. Theoretical calculations on Co(II)-semiquinonate

12a. Discussion of calculation details for Co(II)-semiquinonate

To investigate the effect of a perturbation on the electronic structure of Co(II) by a coupled radical ligand, *ab initio* calculations were undertaken on complexes **3⁺-A** and **3⁺-B**. The active space was selected using the RAS probing technique described by Veryazov *et al.* in which trial orbitals are added into the RAS1 and RAS3 of a minimum active space, minimum basis set calculation (CAS(8,6)) and the trial orbitals are retained if they have natural occupations in the range 0.02–1.98.²⁰ In this method orbitals are included with their antibonding equivalents and care must be taken not to separate degenerate orbitals. In selecting the active space, the five cobalt 3d orbitals were included as well as all eight semiquinonate-based π orbitals, as the inclusion of sufficient π orbitals has been found to be essential in modeling metal-radical interactions.^{19,21,22} Semiquinonate oxygen 2p orbitals were tested and retained along with their antibonding equivalents. The metal-based 3s, 3p, 4d and 4p orbitals and the σ -bonding were trialed and discarded with occupancies less than 0.01 and greater than 1.99. Pyridine π orbitals were trialed and exhibited occupations in the range 0.02–1.98; however, these were ultimately excluded in favor of more relevant orbitals as all excitations were localized on pyridine and including the orbitals did not affect magnetic properties. The final active space of RAS(20,2,2;6,6,5), abbreviated to RAS(20,17), was constructed in the minimal basis and stepwise expanded into the large basis set using the MOLCAS module EXPBAS. The final occupations were 1.037–1.647 for Co 3d orbitals, 0.022–0.048 and 1.954–1.983 for semiquinonate π orbitals and 0.022–0.048 and 1.954–1.983 for O 2p orbitals. Molecular orbitals are shown in Fig. S29–S32 with spin-only state energies reported in Table S14 and spin-orbit state energies reported in Tables 4 (selected) and S14.

12b. Spin-only energies of Co(II)-semiquinonate

Table S14. *Ab initio* RASSCF spin-only energies (cm^{-1}) of **3⁺** with quintet (\mathbb{Q}) or triplet (\mathbb{T}) nature

3⁺-A		3⁺-B	
0	\mathbb{T}	0	\mathbb{T}
19.999	\mathbb{Q}	145.244	\mathbb{Q}
226.124	\mathbb{Q}	254.370	\mathbb{Q}
251.814	\mathbb{T}	362.006	\mathbb{T}
315.498	\mathbb{Q}	434.688	\mathbb{Q}
465.161	\mathbb{T}	576.200	\mathbb{T}

12c. Spin-orbit energies of Co(II)-semiquinonate

Table S15. Simulated spin-orbit energies (cm^{-1}) of $\mathbf{3}^+$ from *ab initio* RASSCF/RASSI-SO and SO+ \mathcal{J} model

<i>Ab initio</i> $\mathbf{3}^+$ -A	<i>Ab initio</i> $\mathbf{3}^+$ -B	SO+ \mathcal{J} $\mathbf{3}^+$ -A	SO+ \mathcal{J} $\mathbf{3}^+$ -B
0	0	0	0
6.587	5.702	7.245	8.225
55.008	33.141	57.626	9.677
63.306	54.142	75.646	52.121
298.415	270.322	321.766	245.472
332.129	311.098	325.857	246.702
356.634	360.14	331.018	298.611
414.558	391.641	331.971	299.977
433.901	431.402	507.265	557.919
481.735	508.658	513.710	560.405
514.605	513.539	548.128	572.758
566.625	598.262	559.495	605.911
956.002	960.544	926.960	941.283
991.428	983.851	927.060	942.046
995.244	984.039	1015.04	977.855
999.519	1013.16	1015.22	979.406
1068.22	1090.14	1170.53	1276.09
1083.44	1101.09	1173.07	1281.36
1087.26	1113.60	1221.43	1284.87
1135.81	1131.69	1242.55	1314.43
1138.35	1141.37	1264.55	1342.23
1160.14	1166.84	1274.57	1350.22
1263.95	1289.35	1276.13	1399.91
1271.70	1294.15	1292.75	1409.43

12d. Composition of spin-orbit states

Table S16. Composition of selected spin-orbit states of **3⁺-A** from *ab initio* RASSCF/RASSI-SO

Spin-Only state	<i>Ms</i>	$ 1_A\rangle$	$ 2_A\rangle$	$ 3_A\rangle$	$ 4_A\rangle$
T_1	-1	6.433	2.042	0.480	18.324
T_1	0	0.417	7.270	1.625	12.048
T_1	1	6.428	2.041	0.480	18.323
T_2	-1	1.122	0.846	2.075	8.115
T_2	0	0.469	1.004	2.448	11.822
T_2	1	1.121	0.845	2.075	8.115
T_3	-1	0.723	0.459	2.068	6.897
T_3	0	0.835	0.264	1.232	4.830
T_3	1	0.723	0.459	2.066	6.897
Q_1	-2	4.782	8.784	6.107	0.443
Q_1	-1	10.632	11.970	2.795	0.306
Q_1	0	11.415	0.452	21.282	0.451
Q_1	1	10.631	11.971	2.794	0.306
Q_1	2	4.781	8.784	6.104	0.442
Q_2	-2	4.397	10.175	7.813	0.373
Q_2	-1	6.740	0.928	4.117	0.252
Q_2	0	1.960	4.307	1.142	0.065
Q_2	1	6.740	0.927	4.117	0.251
Q_2	2	4.398	10.178	7.818	0.373
Q_3	-2	1.379	3.890	3.171	0.082
Q_3	-1	2.682	2.445	7.327	0.328
Q_3	0	7.129	3.629	0.366	0.552
Q_3	1	2.680	2.444	7.325	0.328
Q_3	2	1.377	3.887	3.170	0.082

Table S17. Composition of selected spin-orbit states of **3⁺-B** from *ab initio* RASSCF/RASSI-SO

Spin-Only state	<i>Ms</i>	$ 1_B\rangle$	$ 2_B\rangle$	$ 3_B\rangle$	$ 4_B\rangle$
T ₁	-1	9.558	5.133	22.369	0.867
T ₁	0	0.364	9.733	9.507	0.755
T ₁	1	9.563	5.131	22.369	0.866
T ₂	-1	1.468	1.479	4.523	2.320
T ₂	0	0.017	2.147	11.711	0.529
T ₂	1	1.466	1.480	4.518	2.321
T ₃	-1	1.248	0.692	6.404	0.855
T ₃	0	0.866	0.399	2.942	2.192
T ₃	1	1.248	0.691	6.406	0.855
Q ₁	-2	3.705	9.378	0.363	9.091
Q ₁	-1	10.301	7.224	1.472	1.182
Q ₁	0	7.462	0.043	0.000	17.158
Q ₁	1	10.301	7.227	1.473	1.182
Q ₁	2	3.707	9.381	0.363	9.091
Q ₂	-2	2.558	7.736	0.889	8.496
Q ₂	-1	5.404	2.299	0.703	7.472
Q ₂	0	7.618	3.894	0.001	0.066
Q ₂	1	5.402	2.297	0.703	7.475
Q ₂	2	2.560	7.732	0.888	8.500
Q ₃	-2	1.116	4.212	0.425	4.451
Q ₃	-1	3.841	2.248	0.082	4.728
Q ₃	0	5.258	2.977	1.395	0.363
Q ₃	1	3.842	2.250	0.082	4.730
Q ₃	2	1.115	4.215	0.425	4.451

12e. Fitting of *ab initio* RASSCF/RASSI-SO simulation to SO+ \mathcal{J} model

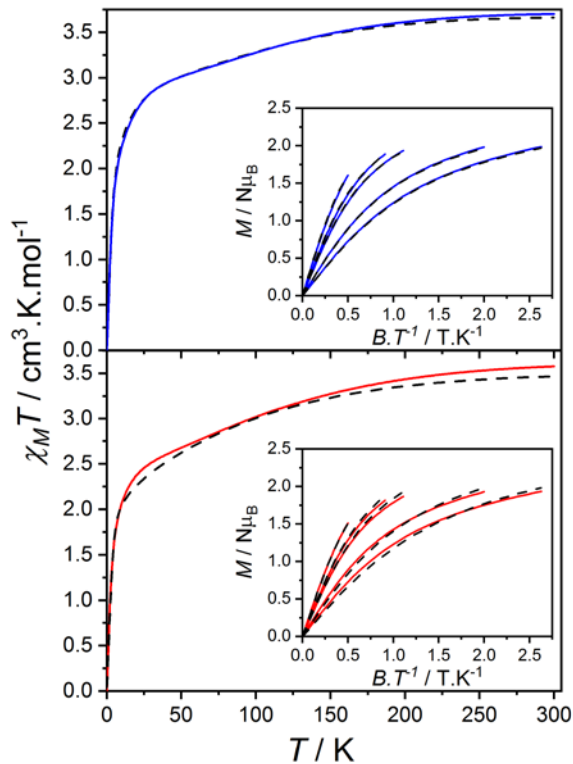


Fig. S28. *Ab initio* RASSCF/RASSI-SO simulation of $\chi_M T$ versus T for **3^{+-A}** (top, blue) and **3^{+-B}** (bottom, red) with inset: M versus B/T at 1.9, 2.5, 4.5, 5.5 and 10 K using the large basis set and RAS(20,17) active space. Overlaid fits using the SO+ \mathcal{J} model, Equation 2 and 3 from the program PHI (black dashed).²³

12f. Optimized orbitals for Co(II)-semiquinonate

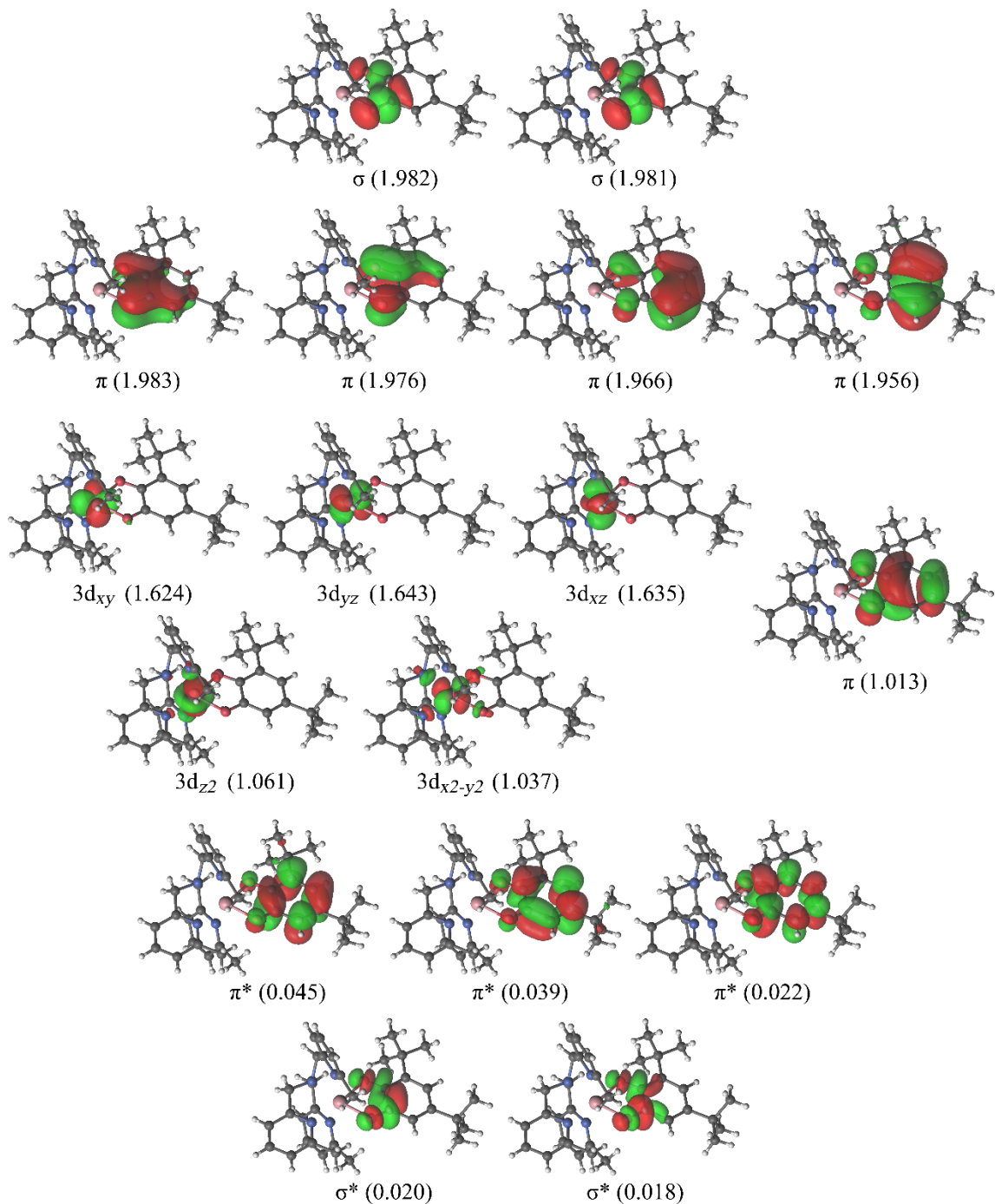


Fig. S29. Active orbitals for quintet **3⁺-A** for the RAS(20,2,2;6,6,5) active space and large basis set. The contour values are ± 0.03 e/au³. Orbitals are labelled by predominant character and natural occupation numbers are given within parentheses.

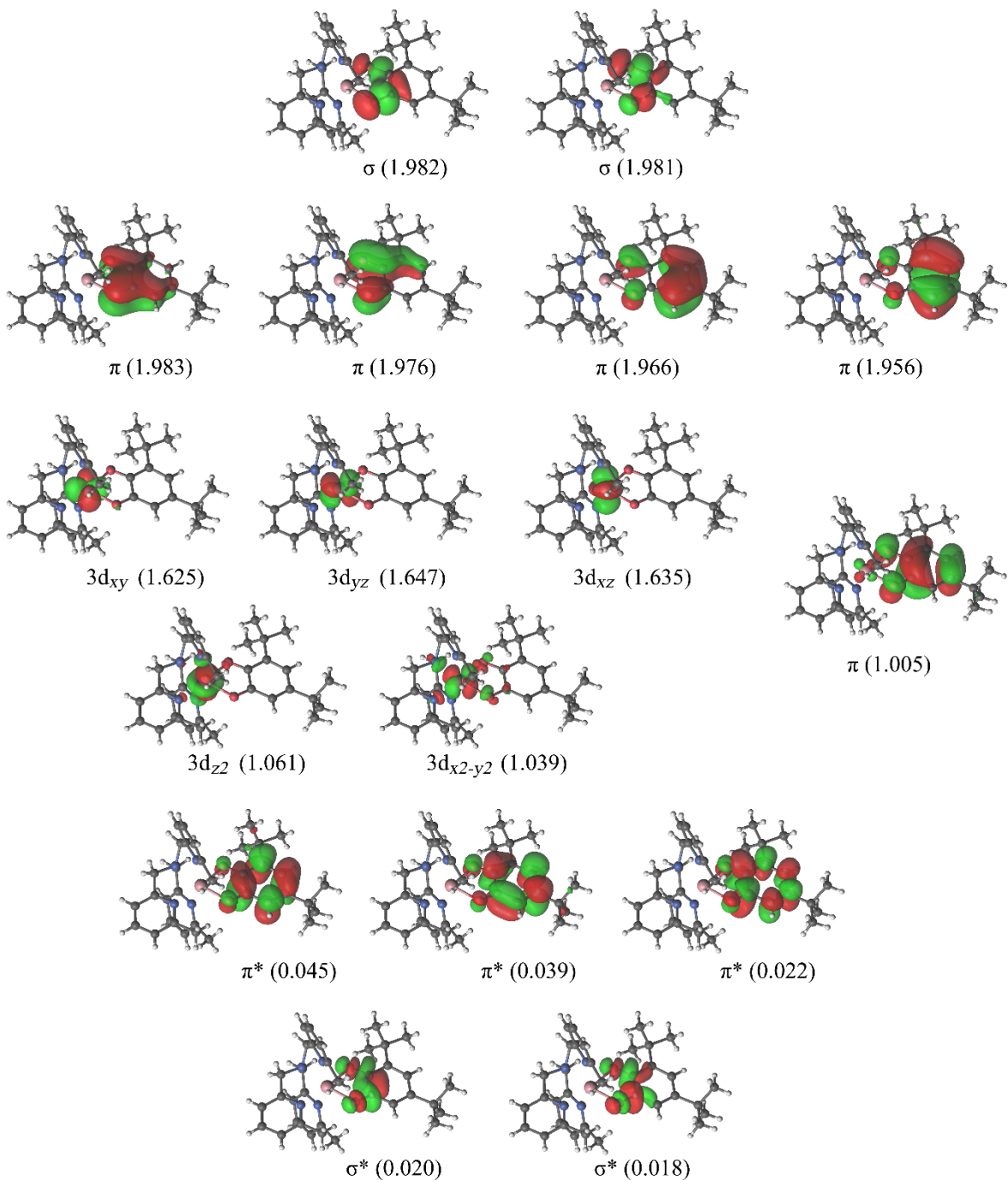


Fig. S30. Active orbitals for triplet **3⁺-A** for the RAS(20,2,2;6,6,5) active space and large basis set. The contour values are ± 0.03 e/au³. Orbitals are labelled by predominant character and natural occupation numbers are given within parentheses.

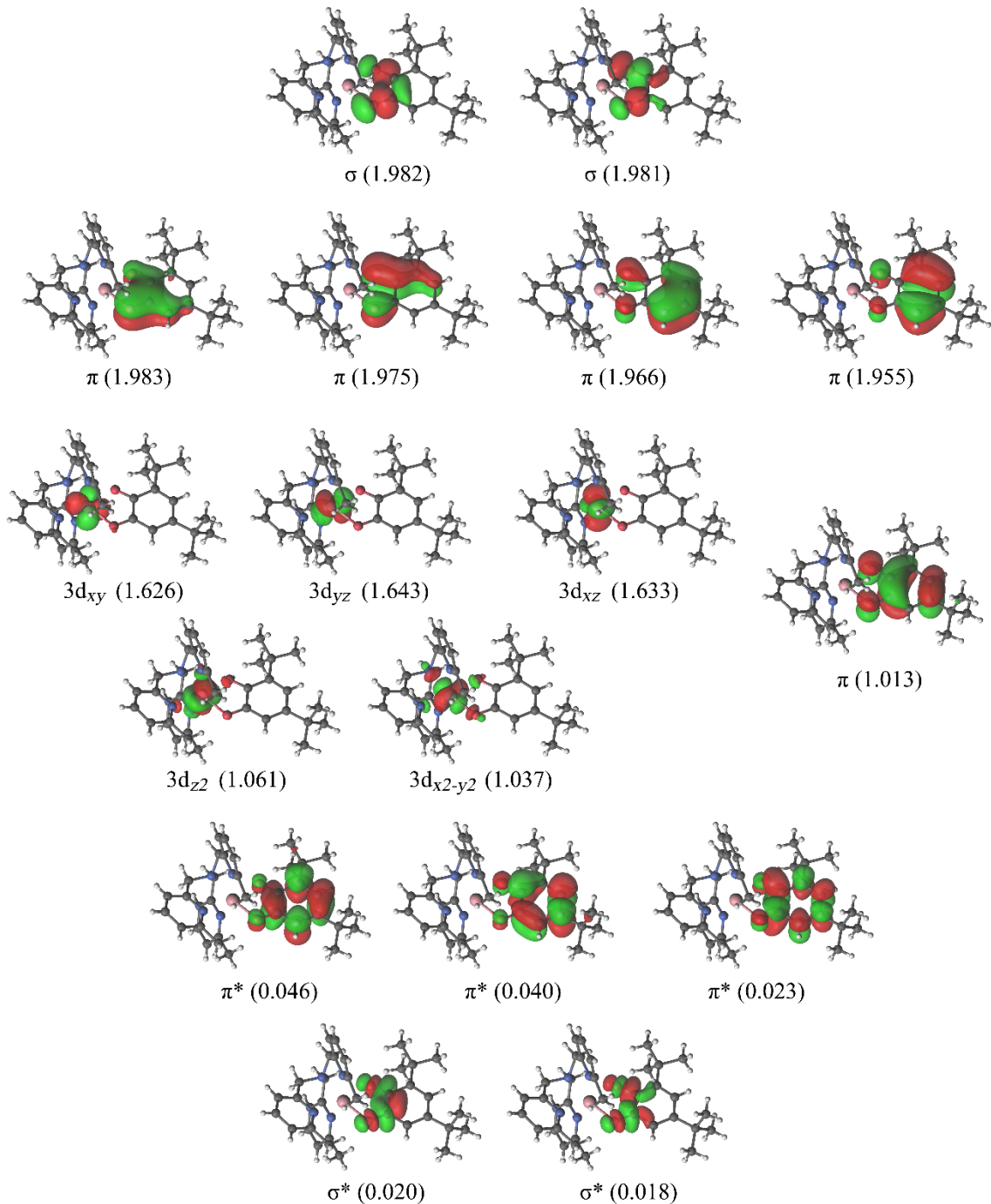


Fig. S31. Active orbitals for quintet **3⁺-B** for the RAS(20,2,2;6,6,5) active space and large basis set. The contour values are ± 0.03 e/au³. Orbitals are labelled by predominant character and natural occupation numbers are given within parentheses.

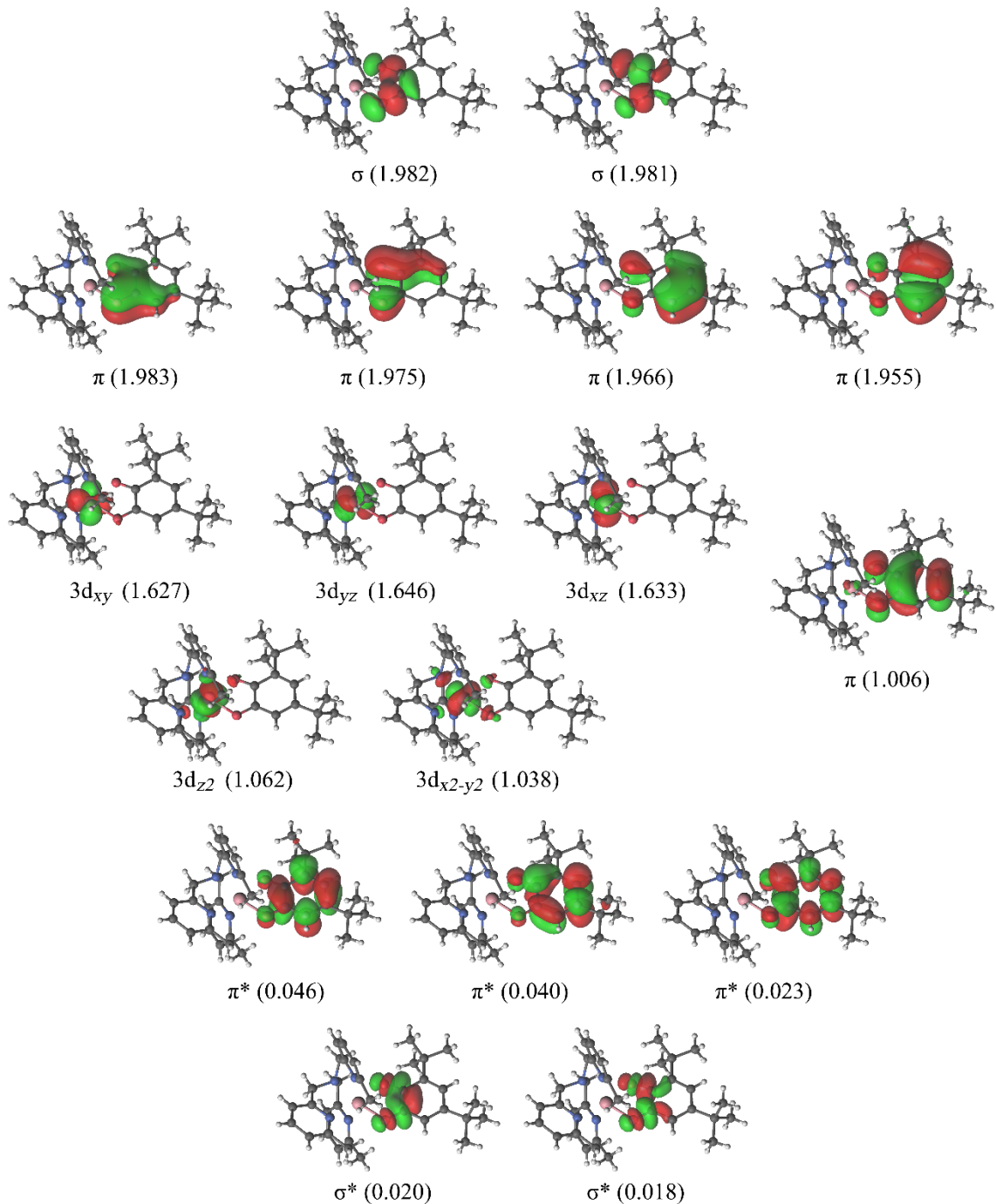


Fig. S32. Active orbitals for triplet **3⁺-B** for the RAS(20,2,2;6,6,5) active space and large basis set. The contour values are ± 0.03 e/au³. Orbitals are labelled by predominant character and natural occupation numbers are given within parentheses.

13. Two-state model of magnetic susceptibility

At 1.9 K, the *ab initio* model indicates that only the first two *pseudo*-doublet RASSCF/RASSI-SO states of **3⁺** have a significant population, and these are well separated from higher energy states. To examine the sensitivity of the *ab initio* magnetic susceptibility to the energy and composition of the ground *pseudo*-doublet, we derive the Van-Vleck susceptibility arising from an isolated *pseudo*-doublet ($\chi_{M1,2a}$, $a = \mathbf{3}^+ \cdot \mathbf{A}$ or $\mathbf{3}^+ \cdot \mathbf{B}$):

$$\chi_{M1,2a} = 2N\mu_B^2 \frac{\mu_{1,2a}^2 \text{avg}}{E_{2a}} \left(\frac{1-\exp\left(\frac{-E_{2a}}{k_B T}\right)}{1+\exp\left(\frac{-E_{2a}}{k_B T}\right)} \right) \quad (\text{S1})$$

where the average transition magnetic moment squared is given by:

$$\mu_{1,2a}^2 \text{avg} = \frac{1}{3} \sum_i^{x,y,z} |\langle 2_a | \hat{\mathbf{L}}_i + 2\hat{\mathbf{S}}_i | 1_a \rangle|^2 \quad (\text{S2})$$

and states $|1_a\rangle$ and $|2_a\rangle$ are the two *ab initio* spin-orbit states of the ground *pseudo*-doublet with energies 0 and E_{2a} . The two-state model is a good approximation (> 92%) of the *ab initio* magnetic susceptibility at 1.9 K for the isolated molecules (Table S18). The two-state magnetic susceptibility is strongly dependent on both the composition of the states ($\mu_{1,2a}^2 \text{avg}$) and their relative energy (E_{2a})—suggesting that one or both are incorrectly reproduced by the *ab initio* calculations, or there is something missing in the *ab initio* model of isolated molecules.

Table S18. Breakdown of contributions to χ at 1.9 K for isolated molecules of **3⁺**

Molecule	Description	E_{2a} / cm ⁻¹	$\mu_{1,2a}^2$ / β^2	$\chi_{M1,2a}$ / cm ³ mol ⁻¹	χ_M / cm ³ mol ⁻¹
Both	Experimental				0.750
3⁺·A	<i>ab initio</i>	6.587	5.404	0.422	0.456
3⁺·B	<i>ab initio</i>	5.702	4.739	0.422	0.439

14. Intermolecular interactions

14a. Intermolecular interaction model

Calculations on molecule **3⁺-A** and **3⁺-B** were performed in the same reference frame as in the crystal, translated so that the Co atom was at the origin in each case. The *ab initio* RASSCF/RASSI-SO wavefunctions obtained for the *pseudo*-doublet for each isolated molecule were represented on the basis of the RASSCF spin-only state, S_{TOT} and M_S for the coupled Co-radical moiety (Tables S16 and S17). The $\widehat{\mathbf{S}}_{sq,i}$ ($i = x,y,z$) operator was constructed on a $\lambda, m_s(\text{Co})$ and $m_s(\text{dbsq})$ basis from the corresponding Pauli matrices in x , y and z -directions (λ is the index labelling one of three RASSCF spin-only states). Under the assumption that the quintet and triplet spin-only states are orthogonal, and using Clebsch-Gordon coefficients, the $\widehat{\mathbf{S}}_{sq,i}$ operators were written on the RASSCF spin-only state, S_{TOT} and M_S basis. The Van-Vleck susceptibility for the exchange states is calculated using:

$$\chi_{EX} = \frac{2N\mu_B^2}{3Z_0} \sum_i^{x,y,z} \sum_n^{1,2,3,4} e^{\frac{-\epsilon_n}{k_B T}} \sum_{m \neq n} \frac{|\langle n_{AB} | \widehat{\mu}_{AB,i} | m_{AB} \rangle|^2}{\epsilon_m - \epsilon_n} \quad (\text{S3})$$

Where the partition function, Z_0 , and $\widehat{\mu}_{AB,i}$ are given by:

$$Z_0 = \sum_n^{1,2,3,4} e^{\frac{-\epsilon_n}{k_B T}} \quad (\text{S4})$$

$$\widehat{\mu}_{AB,i} = \mathbf{T}_{A,i} \otimes \mathbf{I} + \mathbf{I} \otimes \mathbf{T}_{B,i} \quad (\text{S5})$$

Where $\widehat{\mu}_{AB,i}$ operates on the dimer states; \mathbf{I} is the 2×2 identity matrix; and $\mathbf{T}_{A,i}$ and $\mathbf{T}_{B,i}$ are the 2×2 matrices of transition magnetic moments between *ab initio* RASSCF/RASSI-SO

states $|1_A\rangle$ and $|2_A\rangle$ on isolated molecule **3⁺-A** or $|1_B\rangle$ and $|2_B\rangle$ on isolated molecule **3^{+-B}**; and $\hat{\mu}_{AB,i}$ operates on the dimer states. The matrices $\langle n_{AB} | \hat{\mu}_{AB,i} | m_{AB} \rangle$ ($i = x, y, z$) are given below.

$$\begin{aligned}\hat{\mu}_{AB,x} &= \begin{bmatrix} 0 & 2.559 - 3.672i & -0.723 - 0.420i & 0 \\ 2.559 + 3.672i & -0.002 & -0.001i & -3.131 - 1.812i \\ -0.723 + 0.420i & 0.001i & 0 & 0.216 - 0.312i \\ 0 & -3.131 + 1.812i & 0.216 + 0.312i & 0.002 \end{bmatrix} \\ \hat{\mu}_{AB,y} &= \begin{bmatrix} 0 & -0.812 + 1.165i & 0.270 + 0.157i & 0 \\ -0.812 - 1.165i & 0 & 0 & 1.006 + 0.5825i \\ 0.270 - 0.157i & 0 & 0 & -0.036 + 0.052i \\ 0 & 1.006 - 0.5825i & -0.036 - 0.052i & 0 \end{bmatrix} \\ \hat{\mu}_{AB,z} &= \begin{bmatrix} 0 & 2.133 - 3.060i & -0.543 - 0.316i & 0 \\ 2.133 + 3.060i & -0.001 & 0 & -2.591 - 1.500i \\ -0.543 + 0.316i & 0 & 0 & 0.227 - 0.328i \\ 0 & -2.591 + 1.500i & 0.227 + 0.328i & 0.001 \end{bmatrix}\end{aligned}$$

The transition probabilities of INS transitions in a powder sample are given by:

$$p_{n \rightarrow m} = \frac{1}{3} \sum_i^{x,y,z} |\langle n_{AB} | \hat{\mu}_{AB,i} | m_{AB} \rangle|^2 \quad (\text{S6})$$

Table S19. Predicted INS transitions from exchange-coupled dimer states of molecules **3⁺-A** and **3⁺-B** ($J_{AB} = 1.1 \text{ cm}^{-1}$)

	Hot/Cold	Energy / cm ⁻¹	Relative intensity
$ 1_{AB}\rangle \rightarrow 2_{AB}\rangle$	Cold	4.8	9.2
$ 1_{AB}\rangle \rightarrow 3_{AB}\rangle$	Cold	7.8	0.3
$ 1_{AB}\rangle \rightarrow 4_{AB}\rangle$	Cold	12.6	0
$ 2_{AB}\rangle \rightarrow 3_{AB}\rangle$	Hot	2.9	0
$ 2_{AB}\rangle \rightarrow 4_{AB}\rangle$	Hot	7.8	5.9
$ 3_{AB}\rangle \rightarrow 4_{AB}\rangle$	Hot	4.8	0.1

14b. Dipole-dipole interaction

The magnetic dipole interaction, D_{AB} , between two the ground *ab initio* RASSCF/RASSI-SO *pseudo*-doublets of molecules **3⁺-A** and **3⁺-B** can be calculated according to equation S5 for two effective $S = 1/2$ states:²⁴

$$D_{AB} = \frac{\mu_0 \mu_B^2}{4\pi} \sum_{uv} \frac{\rho_u \rho_v}{|r_{uv}|^3} \left(\mathbf{g}_A \cdot \mathbf{g}_B - 3(\mathbf{g}_A \cdot \vec{R}_{uv}) \cdot (\vec{R}_{uv}^T \cdot \mathbf{g}_B) \right) \quad (\text{S7})$$

Where μ_0 is the vacuum permeability in T m A⁻¹, μ_B is the Bohr magneton in J T⁻¹, u and v label atoms of molecule **3⁺-A** and **3⁺-B** respectively, ρ_u and ρ_v are the fractional Mulliken spin density for atom u and v respectively, \mathbf{g}_A and \mathbf{g}_B are the *g*-tensors for the effective $S = 1/2$ doublet on molecule **3⁺-A** or **3⁺-B** respectively, r_{uv} is the distance between atoms u and v in m and \vec{R}_{uv} is the directional unit vector between atoms u and v . The magnetic axes for the *pseudo*-doublet of molecule **3⁺-A** are taken as the common coordinate system, and g_z for the two molecules are assumed to be parallel, consistent with the small angle between them ($\theta = 1.8^\circ$). This results in \mathbf{g}_A and \mathbf{g}_B being 3×3 matrices with only one non-zero component zz , equal to g_z . Equation S5 is simplified by only summing over atoms with significant positive spin

density (Co, O1-O2, N1-N4, C1-C5). The fractional Mulliken spin density is calculated from the *ab initio* RAS(20,17) results, evaluated as the Mulliken spin population on that atom divided by the sum of the populations for Co, O1-O2, N1-N4 and C1-C5. The resulting D_{AB} matrix has only one non-zero component, the zz component.

15. Input coordinates for theoretical calculations

Table S20. Cartesian Coordinates (\AA) for the atoms for **1**, used in the *ab initio* calculations

Co	0.00000000	0.00000000	0.00000000
O	1.98486714	0.00000000	0.00000000
O	0.26370845	2.04381501	-0.00000000
N	-2.10475177	0.25328218	0.19005734
N	-0.63288516	-2.12161449	-0.25984325
N	-0.34539695	-0.05774711	2.22512469
N	-0.65197015	0.03543376	-2.17049471
Br	0.80289696	5.03605750	0.14002050
Br	4.02851809	5.64968748	0.56984735
Br	6.14920046	3.11547229	0.77693361
Br	4.98028923	-0.00074587	0.46771093
C	2.46204879	1.21260639	0.16093347
C	1.52333908	2.31891186	0.13480771
C	2.04776205	3.61086373	0.25073261
C	3.41490690	3.86353184	0.44099508
C	4.29922098	2.79941885	0.51903497
C	3.80904424	1.49071480	0.37098061
C	0.07820930	-3.13120578	-0.79582114
C	-0.53849621	-4.13594420	-1.54196917
C	-1.90698233	-4.11685974	-1.72455408
C	-2.64847101	-3.11033022	-1.12244170
C	-1.97723594	-2.14373695	-0.39257945
C	-2.72958720	-1.07789529	0.36096984
C	0.40960443	-0.53687635	3.23183120
C	0.05700334	-0.33695372	4.56979429
C	-1.11622042	0.32019933	4.87444380
C	-1.92502535	0.76675154	3.83806129
C	-1.49512607	0.57719691	2.53661453
C	-2.29641993	1.10501465	1.37948950
C	-0.01746220	-0.39094275	-3.28041130
C	-0.70148684	-0.52531737	-4.49409792
C	-2.03801413	-0.24070030	-4.56282866
C	-2.69455173	0.20403214	-3.42746623
C	-1.96730557	0.34207185	-2.26104171
C	-2.57966855	0.93467252	-1.02111044
C	1.55624361	-3.15805053	-0.52678788

C	1.62846288	-1.32849582	2.87159833
C	1.43634778	-0.72591348	-3.18599953
H	-0.01761914	-4.83206925	-1.92435731
H	-2.33352381	-4.78127271	-2.25288657
H	-3.59457284	-3.08499647	-1.20844858
H	-3.66404050	-1.04459631	0.03632624
H	-2.74987343	-1.30903254	1.32343975
H	0.62163155	-0.65224471	5.26545860
H	-1.36669596	0.46533852	5.77933265
H	-2.75513198	1.19287916	4.01868394
H	-2.01126235	2.03074820	1.17312383
H	-3.25605715	1.12488977	1.62170240
H	-0.23590714	-0.81493269	-5.27039952
H	-2.51037312	-0.34669635	-5.37982371
H	-3.62125773	0.40908911	-3.44989852
H	-2.34851115	1.89582803	-0.96916684
H	-3.56544719	0.86026283	-1.07464920
H	1.88841901	-2.24048054	-0.43320249
H	1.72803695	-3.65376494	0.30088028
H	2.01507158	-3.59786721	-1.27229854
H	2.05961054	-0.92729189	2.08855051
H	1.36959798	-2.25127536	2.66454488
H	2.25438218	-1.32581169	3.62650088
H	1.80774207	-0.33924533	-2.36655737
H	1.90662895	-0.35895076	-3.96347473
H	1.54711645	-1.70025374	-3.16722018

Table S23. Cartesian Coordinates (Å) for the atoms for **2⁺-I** used in the *ab initio* calculations

Co	0.00000000	0.00000000	0.00000000
O	2.02369489	0.00000000	0.00000000
O	0.42943349	2.03242908	0.00000000
N	-2.07431685	0.44249233	0.15613853
N	-0.73778358	-2.03490159	-0.09865348
N	-0.31090350	0.14071731	2.20679510
N	-0.58242126	0.00250857	-2.16510037
C	2.56545667	1.13643979	0.25466361
C	1.64857473	2.29829225	0.26697205
C	2.00915625	3.62541810	0.57970550
C	3.23831965	4.18813195	0.88301571
C	4.49659397	3.59741360	0.95343974
C	4.79630100	2.25893539	0.78512565
C	3.94889667	1.18968289	0.50973644
C	-0.07610813	-3.16525878	-0.43843580
C	-0.74882345	-4.27260715	-0.94671195
C	-2.11866362	-4.23252548	-1.10159300
C	-2.79988496	-3.09358897	-0.71362124
C	-2.08676717	-2.02851714	-0.20439672
C	-2.80781040	-0.82619958	0.35298593
C	0.45487517	-0.29859751	3.23227981
C	0.14237896	0.02027807	4.55284274
C	-0.99450174	0.75410955	4.83554942
C	-1.80705897	1.15995335	3.78535207
C	-1.42097011	0.85047332	2.49267287
C	-2.23595081	1.34184572	1.31563947
C	0.02125539	-0.56830383	-3.21978658
C	-0.66237430	-0.80095965	-4.41324950
C	-1.99570638	-0.45321514	-4.51653629
C	-2.61205414	0.15656008	-3.44015341
C	-1.88054997	0.37629477	-2.29363783
C	-2.45652643	1.10365486	-1.10750180
C	1.40310481	-3.21015494	-0.20589697
C	1.64261481	-1.15654342	2.91446380
C	1.46240226	-0.95113439	-3.08927047
H	1.28438011	4.23881613	0.58258302
H	3.22019254	5.11874741	1.07155465
H	5.22746992	4.17671573	1.13712740
H	5.71545168	2.03582517	0.86952245
H	4.38180612	0.34376170	0.49032732
H	-0.26558801	-5.05355641	-1.18609531
H	-2.58536762	-4.97502962	-1.46872539
H	-3.74486326	-3.04587914	-0.79650972
H	-3.69469916	-0.75448496	-0.08063803
H	-2.95731511	-0.96297362	1.32275102
H	0.71027784	-0.26690401	5.25883524
H	-1.21576849	0.97748497	5.73262235
H	-2.60976823	1.63941377	3.95004963
H	-3.19175127	1.38371033	1.56997065

H	-1.94387639	2.25474980	1.06879217
H	-0.21381448	-1.19537848	-5.15096667
H	-2.48129815	-0.63139182	-5.31410811
H	-3.52281363	0.41968228	-3.49074230
H	-2.12878762	2.03862777	-1.10273849
H	-3.44251553	1.12536215	-1.18250520
H	1.76185585	-2.29856007	-0.20481064
H	1.83031856	-3.72856730	-0.91909513
H	1.58542739	-3.63400511	0.65907946
H	1.34831653	-1.95617128	2.42885721
H	2.08488835	-1.42505156	3.74726392
H	2.27159016	-0.65011446	2.35887555
H	1.86844934	-0.45129405	-2.35073863
H	1.93262002	-0.74092430	-3.92268951
H	1.53050234	-1.91254739	-2.90979657

Table S21. Cartesian Coordinates (Å) for the atoms for **2⁺-IIA** used in the *ab initio* calculations

Co	0.00000000	0.00000000	0.00000000
O	2.01542492	0.00000000	0.00000000
O	0.41549230	2.02446141	0.00000000
N	-2.06862321	0.43975333	0.14498907
N	-0.74935053	-2.03136072	-0.26167036
N	-0.35186893	-0.00225164	2.18126423
N	-0.55071853	0.14060115	-2.17336356
C	2.56934250	1.16404562	0.09512764
C	1.64880811	2.31293432	0.08059462
C	2.00381672	3.68512334	0.15075034
C	3.24526887	4.27945516	0.22785267
C	4.49075498	3.71458780	0.29356659
C	4.79936776	2.38471503	0.31647839
C	3.96189959	1.25776380	0.22735059
C	-0.09331574	-3.09602756	-0.75231976
C	-0.77045887	-4.11607228	-1.41600322
C	-2.13815751	-4.06112452	-1.54487349
C	-2.82273951	-2.99234834	-1.00009426
C	-2.09479051	-1.99645447	-0.37083657
C	-2.80235007	-0.84061433	0.29684933
C	0.35573199	-0.56832381	3.17812884
C	-0.05252826	-0.42962726	4.51132443
C	-1.19963269	0.25906182	4.80408690
C	-1.93460086	0.82312379	3.78742132
C	-1.47481777	0.67949899	2.48863175
C	-2.21739471	1.29350560	1.33504957
C	0.09682561	-0.29823125	-3.26108725
C	-0.53642146	-0.31720141	-4.51078016
C	-1.81825684	0.07749895	-4.63397445
C	-2.49761437	0.52796560	-3.52008287
C	-1.82587753	0.56500134	-2.30609193
C	-2.46106454	1.16422854	-1.08556158
C	1.38311275	-3.19142389	-0.53440087
C	1.55647681	-1.38040569	2.80999743
C	1.51040775	-0.75067763	-3.12896212
H	1.27063045	4.28894952	0.14362963
H	3.23491082	5.22899939	0.23689810
H	5.22425241	4.31631199	0.32794173
H	5.72505145	2.18993679	0.40739456
H	4.41538876	0.42363864	0.26268376
H	-0.28789437	-4.84864316	-1.77815943
H	-2.60614681	-4.74900641	-2.00344571
H	-3.76947165	-2.94081544	-1.05522468
H	-3.70691620	-0.74430387	-0.09523823
H	-2.90928411	-1.03974341	1.25999211
H	0.46435098	-0.81285622	5.20921282
H	-1.48641996	0.34673666	5.70564251
H	-2.73533043	1.29846030	3.97117358
H	-1.85659559	2.19673967	1.14661136

H	-3.17568012	1.38397010	1.56412366
H	-0.05766880	-0.61114594	-5.27722435
H	-2.25063345	0.04799500	-5.47893639
H	-3.40336048	0.80567192	-3.58204788
H	-2.18946171	2.11361655	-1.00787151
H	-3.44568007	1.13570643	-1.18223073
H	1.74296188	-2.29997706	-0.33779259
H	1.81132954	-3.54547673	-1.34167237
H	1.56384589	-3.79003387	0.22101899
H	1.27341874	-2.17876907	2.31799267
H	2.03165174	-1.64788182	3.62361195
H	2.15252474	-0.84464140	2.24620435
H	1.81998650	-0.58851286	-2.21273048
H	2.07251768	-0.25146397	-3.75706831
H	1.56678503	-1.70807325	-3.32849217

Table S22. Cartesian Coordinates (Å) for the atoms for **2⁺-IIB** used in the *ab initio* calculations

Co	0.00000000	0.00000000	0.00000000
O	1.99571333	0.00000000	0.00000000
O	0.41966631	2.04410469	0.00000000
N	-2.07362373	0.39762914	-0.11044995
N	-0.65040958	-2.06174131	-0.17875761
N	-0.55115792	0.08936385	2.13830513
N	-0.38776140	-0.00480835	-2.25659555
C	2.56608389	1.14697981	-0.09323908
C	1.66630429	2.30957928	-0.09321369
C	2.07391771	3.66203481	-0.17538713
C	3.34012258	4.21918188	-0.31057134
C	4.57708819	3.60855328	-0.41950878
C	4.84658597	2.26168753	-0.35002530
C	3.97200693	1.18724723	-0.17852030
C	0.07940415	-3.18017714	-0.36719090
C	-0.49179223	-4.32716274	-0.91627322
C	-1.80804877	-4.31978117	-1.30711711
C	-2.56631971	-3.17610433	-1.09353465
C	-1.96260209	-2.08291622	-0.49865788
C	-2.80233177	-0.89601894	-0.10390006
C	0.11543947	-0.35585956	3.22059768
C	-0.41488634	-0.19247891	4.50628141
C	-1.63881864	0.42780340	4.67318211
C	-2.32992272	0.86464925	3.55561987
C	-1.75281537	0.68209787	2.30462816
C	-2.43135409	1.19884860	1.07332776
C	0.31402148	-0.52612365	-3.28584823
C	-0.17165769	-0.47179626	-4.58624628
C	-1.40897626	0.06717781	-4.83886855
C	-2.14661151	0.57473215	-3.79007487
C	-1.59394415	0.53694738	-2.51842244
C	-2.29860974	1.16362993	-1.34975262
C	1.52362081	-3.17580460	0.02948687
C	1.43996562	-1.01314176	3.00993742
C	1.61773895	-1.19192811	-3.00009188
H	1.36572012	4.29294530	-0.13092624
H	3.35926724	5.16988014	-0.33189304
H	5.32166885	4.18246923	-0.55808599
H	5.76340345	2.02816046	-0.43127452
H	4.39643355	0.33947677	-0.10690338
H	0.03032308	-5.11441681	-1.02077448
H	-2.19472893	-5.08500308	-1.71604897
H	-3.47963063	-3.14528101	-1.35045679
H	-3.57042116	-0.83113422	-0.72538326
H	-3.16363499	-1.05125664	0.80506674
H	0.06664301	-0.50866486	5.26203080
H	-2.00156816	0.55245852	5.54257179
H	-3.17948366	1.27989886	3.64246792
H	-2.16726326	2.14153249	0.92366090

H	-3.41294498	1.17397001	1.20309885
H	0.35345730	-0.80756458	-5.30362172
H	-1.75281183	0.08948638	-5.72413849
H	-3.01062793	0.94118274	-3.93534549
H	-1.96946791	2.08985602	-1.22655872
H	-3.26908153	1.20645753	-1.53733012
H	1.82760751	-2.25089316	0.14747765
H	2.05591517	-3.60722938	-0.67068899
H	1.63275471	-3.66578532	0.87109861
H	1.31347956	-1.85565541	2.52603669
H	1.85690765	-1.19515496	3.87709079
H	2.01978042	-0.42001817	2.48699267
H	2.05580183	-0.74356509	-2.24723663
H	2.19271449	-1.13868707	-3.79188256
H	1.46090638	-2.13239311	-2.77252646

Table S24. Cartesian Coordinates (Å) for the atoms for **2⁺-III** used in the *ab initio* calculations

Co	0.00000000	0.00000000	0.00000000
O	1.99587784	0.00000000	0.00000000
O	0.41014090	2.05011497	0.00000000
N	-2.08480938	0.32947188	-0.11518325
N	-0.61708762	-2.08528254	-0.30599879
N	-0.57134986	0.06158386	2.11675007
N	-0.36909645	0.00636714	-2.27060311
C	2.55696428	1.14735078	-0.21040694
C	1.65247948	2.31137783	-0.19531870
C	2.06086988	3.64911770	-0.35909843
C	3.30828288	4.20471465	-0.57890508
C	4.54548016	3.59458449	-0.73276023
C	4.80138140	2.23562136	-0.69419879
C	3.93262326	1.17628711	-0.47153480
C	0.16202033	-3.11948486	-0.67671356
C	-0.33246348	-4.12457324	-1.52285538
C	-1.63908717	-4.07570431	-1.94425177
C	-2.45906858	-3.06460370	-1.48556886
C	-1.91821087	-2.09093257	-0.67260406
C	-2.76611404	-0.98131539	-0.09693778
C	0.10827415	-0.36515197	3.20388042
C	-0.41618745	-0.19578360	4.48100222
C	-1.63584454	0.40979535	4.66575844
C	-2.34833530	0.81475464	3.54108724
C	-1.78102505	0.62893633	2.29230784
C	-2.47185726	1.13477762	1.05367382
C	0.32928384	-0.55297184	-3.27683242
C	-0.22806004	-0.69711980	-4.55224774
C	-1.51775385	-0.29714688	-4.78297862
C	-2.23937374	0.27255347	-3.74633063
C	-1.63074561	0.41590203	-2.51987520
C	-2.33796554	1.07834817	-1.36372212
C	1.54184006	-3.19442607	-0.12535287
C	1.43358134	-1.01794943	2.98851193
C	1.71584170	-1.06056131	-3.01818824
H	1.35452845	4.28251931	-0.30998093
H	3.32023073	5.15286749	-0.63421311
H	5.29075693	4.16653664	-0.87931539
H	5.70658657	1.99127599	-0.84306355
H	4.34373245	0.32032963	-0.50077440
H	0.23319391	-4.83536783	-1.80245537
H	-1.97436461	-4.73017966	-2.54547423
H	-3.37858729	-3.04039124	-1.72561482
H	-3.00372740	-1.20894485	0.83725297
H	-3.60787564	-0.91571933	-0.61544827
H	0.07470284	-0.50272578	5.23385546
H	-1.98332855	0.54786997	5.53864979
H	-3.20786207	1.21097326	3.62982198
H	-2.22631220	2.08178103	0.89957046

H	-3.45252442	1.08743282	1.17768895
H	0.28771534	-1.07030733	-5.25642107
H	-1.91139700	-0.40959042	-5.64002539
H	-3.13649540	0.55824933	-3.87880507
H	-3.31175424	1.10797165	-1.54180952
H	-2.01488335	2.00849761	-1.26526271
H	1.51086267	-3.56189562	0.78194740
H	2.09076154	-3.77396924	-0.69430412
H	1.93325466	-2.29574726	-0.10138063
H	1.96350943	-0.48161522	2.36186856
H	1.90736077	-1.08336969	3.84344935
H	1.29869287	-1.91486895	2.61884520
H	1.69471536	-2.03642416	-2.92665215
H	2.29869545	-0.81428202	-3.76538688
H	2.06035104	-0.66362646	-2.19131474

Table S25. Cartesian Coordinates (Å) for the atoms for **2⁺-IV** used in the *ab initio* calculations

Co	0.00000000	-0.00000000	0.00000000
O	2.00211310	0.00000000	0.00000000
O	0.42349539	2.04577994	-0.00000000
N	-2.08661716	0.40440827	0.09501301
N	-0.69406315	-2.06413381	-0.06688475
N	-0.36516520	0.13324521	2.17615568
N	-0.49983087	-0.00483746	-2.15838267
C	2.56548861	1.14155073	0.14364010
C	1.66010189	2.31106667	0.16563660
C	2.06391779	3.64068205	0.37158120
C	3.31557007	4.19550279	0.59967735
C	4.56434717	3.58366569	0.64312090
C	4.83535256	2.23821041	0.47946087
C	3.96630647	1.17779937	0.26335881
C	-0.01095709	-3.20208640	-0.29192262
C	-0.67591995	-4.38495830	-0.60292015
C	-2.04834124	-4.39655980	-0.72038061
C	-2.73610894	-3.23686832	-0.46998869
C	-2.04370651	-2.09664367	-0.13507918
C	-2.81204865	-0.86866137	0.28641955
C	0.38901847	-0.29040290	3.21062470
C	0.05707523	0.03583809	4.52612179
C	-1.08886771	0.75240739	4.78669344
C	-1.89288779	1.13786014	3.72193536
C	-1.48646362	0.82981857	2.44227716
C	-2.28114979	1.31022108	1.24312037
C	0.17028103	-0.54597746	-3.18786980
C	-0.45909625	-0.76834333	-4.41627523
C	-1.77295355	-0.42489884	-4.58800624
C	-2.45900876	0.16859745	-3.53570700
C	-1.79134252	0.35856696	-2.34944791
C	-2.44036690	1.05936592	-1.18025937
C	1.47820372	-3.20043479	-0.17352515
C	1.58895730	-1.13155655	2.91632359
C	1.61341354	-0.89364987	-2.99625541
H	1.35365882	4.27265937	0.35217059
H	3.32000295	5.13437356	0.74809097
H	5.30970233	4.15019555	0.80156771
H	5.75547952	2.00449565	0.52167584
H	4.39087788	0.33192749	0.18209255
H	-0.18250755	-5.18625492	-0.73582478
H	-2.50745655	-5.19022942	-0.96937670
H	-3.68418261	-3.22228495	-0.52710428
H	-3.65688262	-0.83167397	-0.22955261
H	-3.04951393	-0.95643748	1.24329807
H	0.62111350	-0.23532919	5.24053154
H	-1.32524867	0.98032065	5.67831844
H	-2.70634225	1.60434393	3.87374717
H	-3.24202872	1.34625389	1.47628939

H	-1.98951496	2.22361823	0.99755119
H	0.02579933	-1.15931980	-5.13416797
H	-2.21036992	-0.59000364	-5.41474545
H	-3.36523307	0.43553651	-3.63357471
H	-2.14542478	2.00433537	-1.15767084
H	-3.42398894	1.04823642	-1.29428926
H	1.79447698	-2.28122071	-0.05133756
H	1.87061687	-3.57549344	-0.99102054
H	1.74499648	-3.74380675	0.59599646
H	1.30212707	-1.98399743	2.52781635
H	2.08151243	-1.30125799	3.74648654
H	2.16904553	-0.66174151	2.28130119
H	2.16315626	-0.09583810	-3.13753237
H	1.87137741	-1.58630219	-3.64067916
H	1.74937217	-1.22917617	-2.08603884

Table S26. Cartesian Coordinates (\AA) for the atoms for **3⁺-A**, used in **3⁺-A** and **3-A** *ab initio* calculations

Co	0.000000	0.000000	0.000000
O	-0.730116	0.088591	-1.888733
O	-1.927691	0.679200	0.358565
N	0.347618	-0.005716	2.089353
N	1.993338	-0.798592	-0.085351
N	0.874450	2.029343	0.366704
N	-0.575510	-2.127460	0.584482
C	-1.977770	0.396279	-1.952306
C	-2.648018	0.744929	-0.699311
C	-4.035071	1.136762	-0.725268
C	-4.664561	1.123108	-1.943727
H	-5.563855	1.359669	-1.969905
C	-4.034054	0.768426	-3.178465
C	-2.708689	0.412473	-3.167026
H	-2.286146	0.178453	-3.962907
C	-4.735525	1.558444	0.569524
C	-6.204205	1.941069	0.329967
H	-6.246750	2.680600	-0.280472
H	-6.609829	2.188426	1.162585
H	-6.673573	1.191378	-0.042896
C	-4.005618	2.779670	1.162805
H	-3.086578	2.556763	1.323169
H	-4.423910	3.029885	1.989703
H	-4.053728	3.512532	0.544446
C	-4.707964	0.392151	1.568445
H	-5.184246	-0.355000	1.199981
H	-5.124024	0.664276	2.390063
H	-3.798217	0.140349	1.738928
C	-4.877521	0.800814	-4.453678
C	-4.030866	0.550282	-5.702055
H	-3.328968	1.204079	-5.749130
H	-4.584012	0.619821	-6.483857
H	-3.646964	-0.329598	-5.656739
C	-5.541953	2.175408	-4.607223
H	-6.133476	2.328140	-3.866117
H	-6.042108	2.197952	-5.425762
H	-4.867045	2.858418	-4.625041
C	-5.946880	-0.290224	-4.368327
H	-5.523207	-1.152004	-4.336870
H	-6.516395	-0.240689	-5.139790
H	-6.470503	-0.164481	-3.573546
C	2.697182	-1.265045	-1.144106
C	3.889429	-1.956629	-0.952285
H	4.376449	-2.260189	-1.683933
C	4.344187	-2.190014	0.325128
H	5.129580	-2.669804	0.460854
C	3.631432	-1.710224	1.404781

H	3.928552	-1.856924	2.273475
C	2.469356	-1.008797	1.165225
C	1.754509	-0.387388	2.344748
H	1.774202	-1.015466	3.082995
H	2.243788	0.403900	2.621040
C	1.545463	2.854607	-0.464154
C	2.161241	4.016137	0.019798
H	2.609516	4.582613	-0.564244
C	2.101871	4.316522	1.359905
H	2.515753	5.081137	1.688333
C	1.420972	3.471253	2.217160
H	1.368250	3.655421	3.126990
C	0.815058	2.339571	1.679754
C	0.073380	1.373958	2.558127
H	0.363740	1.473981	3.478955
H	-0.878476	1.553364	2.517651
C	-0.672651	-3.251522	-0.153545
C	-0.854457	-4.501325	0.449416
H	-0.955631	-5.260860	-0.078092
C	-0.883382	-4.606428	1.821640
H	-0.980432	-5.435503	2.229479
C	-0.766038	-3.456647	2.584524
H	-0.773077	-3.498561	3.514152
C	-0.638022	-2.239232	1.929649
C	-0.602291	-0.951324	2.708812
H	-1.488431	-0.558220	2.726630
H	-0.333063	-1.129777	3.624141
C	2.194517	-1.022769	-2.535908
H	1.257322	-0.815421	-2.506651
H	2.332422	-1.809294	-3.067596
H	2.671681	-0.285143	-2.924610
C	1.657479	2.476745	-1.906991
H	2.463700	1.972505	-2.044697
H	1.679984	3.271208	-2.445057
H	0.899976	1.940752	-2.156886
C	-0.538104	-3.157532	-1.639277
H	-0.868205	-2.307818	-1.936908
H	-1.045165	-3.860547	-2.051296
H	0.386128	-3.244536	-1.884113

Table S27. Cartesian Coordinates (Å) for the atoms for **3⁺-B** used in used in **3⁺-B** and **3-B ab***initio* calculations

Co	0.000000	0.000000	0.000000
O	0.867560	-0.181945	1.809101
O	1.935991	-0.622679	-0.543126
N	-0.530302	0.105103	-2.045357
N	-1.954313	0.903060	0.281352
N	-0.997945	-1.950912	-0.329747
N	0.566756	2.141432	-0.565784
C	2.126839	-0.458832	1.775444
C	2.726526	-0.690313	0.459094
C	4.145456	-0.971328	0.376603
C	4.836569	-1.017370	1.563825
H	5.750940	-1.185027	1.522029
C	4.257824	-0.827486	2.862576
C	2.915149	-0.542026	2.943748
H	2.522845	-0.403899	3.774606
C	4.814975	-1.244405	-0.974063
C	6.313207	-1.538439	-0.820299
H	6.744755	-0.791288	-0.402780
H	6.700440	-1.686726	-1.685253
H	6.431330	-2.321789	-0.277392
C	4.162254	-2.479602	-1.623439
H	4.225825	-3.226754	-1.025318
H	4.616099	-2.686950	-2.444178
H	3.237999	-2.293211	-1.806241
C	4.665026	-0.036833	-1.916010
H	3.736416	0.196235	-1.993222
H	5.012007	-0.261010	-2.782944
H	5.152032	0.710636	-1.559865
C	5.155014	-0.907187	4.102153
C	4.344661	-0.958944	5.399365
H	4.941270	-1.035787	6.148171
H	3.755889	-1.718479	5.378247
H	3.826840	-0.156225	5.486036
C	6.029718	-2.160801	4.050238
H	6.590428	-2.128095	3.270856
H	5.470259	-2.940975	4.007783
H	6.577291	-2.201127	4.837100
C	6.023150	0.349285	4.141529
H	5.463793	1.120251	4.258558
H	6.508399	0.428033	3.317051
H	6.641890	0.288319	4.872297
C	-2.528541	1.398091	1.401481
C	-3.633253	2.242407	1.337907
H	-4.024809	2.561844	2.118170
C	-4.142082	2.601218	0.105810
H	-4.858396	3.190556	0.045975
C	-3.575478	2.073481	-1.040277

H	-3.916665	2.288767	-1.878834
C	-2.492506	1.222179	-0.919069
C	-1.942492	0.556951	-2.159526
H	-2.496925	-0.210205	-2.371585
H	-2.009860	1.180582	-2.899533
C	-1.625734	-2.773001	0.532567
C	-2.370069	-3.871342	0.089971
H	-2.803814	-4.420672	0.703710
C	-2.456523	-4.135846	-1.261575
H	-2.932011	-4.874742	-1.568664
C	-1.825182	-3.287402	-2.155566
H	-1.886403	-3.433149	-3.071116
C	-1.101345	-2.218274	-1.654896
C	-0.372618	-1.270760	-2.565606
H	0.568372	-1.505733	-2.602562
H	-0.736680	-1.327916	-3.462677
C	0.737084	3.239138	0.199080
C	0.949314	4.497833	-0.373083
H	1.106258	5.235458	0.169163
C	0.925613	4.640722	-1.744207
H	1.046409	5.476782	-2.136208
C	0.718425	3.516343	-2.530849
H	0.685490	3.584295	-3.458277
C	0.562336	2.291942	-1.905671
C	0.405075	1.029755	-2.715411
H	0.068289	1.250439	-3.599063
H	1.268083	0.599500	-2.820340
C	-1.971193	1.011973	2.737849
H	-2.483085	0.285144	3.099273
H	-2.017210	1.764840	3.332450
H	-1.056301	0.739214	2.637319
C	-1.526801	-2.480555	1.995422
H	-0.714874	-2.001082	2.170965
H	-1.524718	-3.306136	2.487733
H	-2.278586	-1.947102	2.267755
C	0.650196	3.095297	1.686793
H	-0.264803	3.181030	1.964185
H	1.176491	3.781164	2.104971
H	0.984335	2.231611	1.944387

16. References

1. A. Beni, A. Dei, S. Laschi, M. Rizzitano and L. Sorace, *Chem. - Eur. J.*, 2008, **14**, 1804-1813.
2. H. Nagao, N. Komeda, M. Mukaida, M. Suzuki and K. Tanaka, *Inorg. Chem.*, 1996, **35**, 6809-6815.
3. O. Fuentes and W. W. Paudler, *J. Org. Chem.*, 1975, **40**, 1210-1213.
4. G. K. Gransbury, M.-E. Boulon, S. Petrie, R. W. Gable, R. J. Mulder, L. Sorace, R. Stranger and C. Boskovic, *Inorg. Chem.*, 2019, **58**, 4230-4243.
5. M. Llunell, D. Casanova, J. Cirera, P. Alemany and S. Alvarez, SHAPE 2.1, Universitat de Barcelona, Barecelona, Spain, 2013.
6. S. Alvarez, D. Avnir, M. Llunell and M. Pinsky, *New J. Chem.*, 2002, **26**, 996-1009.
7. M. A. Halcrow, *Chem. Soc. Rev.*, 2011, **40**, 4119-4142.
8. C. Janiak, *J. Chem. Soc., Dalton Trans.*, 2000, 3885-3896.
9. M. Nishio, *CrystEngComm*, 2004, **6**, 130-158.
10. A. Bencini, A. Beni, F. Costantino, A. Dei, D. Gatteschi and L. Sorace, *Dalton Trans.*, 2006, 722-729.
11. S. Harmalker, S. E. Jones and D. T. Sawyer, *Inorg. Chem.*, 1983, **22**, 2790-2794.
12. L. Banci, A. Bencini, C. Benelli, D. Gatteschi and C. Zanchini, in *Structures versus Special Properties*, Springer Berlin Heidelberg, Berlin, Heidelberg, 1982, pp. 37-86.
13. B. S. Parajon-Costa, E. J. Baran, J. Romero, R. Saez-Puche, G. Arrambide and D. Gambino, *J. Coord. Chem.*, 2011, **64**, 57-70.
14. M. Hasegawa, Y. Inomaki, T. Inayoshi, T. Hoshi and M. Kobayashi, *Inorg. Chim. Acta*, 1997, **257**, 259-264.
15. O. Kahn, *Molecular Magnetism*, VCH Publishers, Inc., New York, NY, 1993.
16. R. Herchel, L. Váhovská, I. Potočnák and Z. Trávníček, *Inorg. Chem.*, 2014, **53**, 5896-5898.
17. J. Li, Y. Han, F. Cao, R.-M. Wei, Y.-Q. Zhang and Y. Song, *Dalton Trans.*, 2016, **45**, 9279-9284.
18. J. P. S. Walsh, G. Bowling, A.-M. Ariciu, N. F. M. Jailani, N. F. Chilton, P. G. Waddell, D. Collison, F. Tuna and L. J. Higham, *Magnetochemistry*, 2016, **2**, 23.
19. S. Vancoillie, H. Zhao, V. T. Tran, M. F. A. Hendrickx and K. Pierloot, *J. Chem. Theory Comput.*, 2011, **7**, 3961-3977.
20. V. Veryazov, P. Å. Malmqvist and B. O. Roos, *Int. J. Quantum Chem.*, 2011, **111**, 3329-3338.
21. F. Ortu, J. Liu, M. Burton, J. M. Fowler, A. Formanuk, M.-E. Boulon, N. F. Chilton and D. P. Mills, *Inorg. Chem.*, 2017, **56**, 2496-2505.
22. U. Albold, H. Bamberger, P. P. Hallmen, J. van Slageren and B. Sarkar, *Angew. Chem., Int. Ed.*, 2019, **58**, 9802-9806.

23. N. F. Chilton, R. P. Anderson, L. D. Turner, A. Soncini and K. S. Murray, *J. Comput. Chem.*, 2013, **34**, 1164-1175.
24. M. J. Giansiracusa, E. Moreno-Pineda, R. Hussain, R. Marx, M. Martínez Prada, P. Neugebauer, S. Al-Badran, D. Collison, F. Tuna, J. van Slageren, S. Carretta, T. Guidi, E. J. L. McInnes, R. E. P. Winpenny and N. F. Chilton, *J. Am. Chem. Soc.*, 2018, **140**, 2504-2513.